Title

Insights on the kinematics of the India-Eurasia collision from global geodynamic models

Authors

Sabin Zahirovic[a,*], R Dietmar Müller[a], Maria Seton[a], Nicolas Flament[a], Michael Gurnis[b], Joanne Whittaker[a]

[a] EarthByte Group, School of Geosciences, The University of Sydney, Sydney, NSW 2006, Australia

[b] Seismological Laboratory, California Institute of Technology, Pasadena, CA 91125, USA

[*] Corresponding author. E-mail address: sabin.zahirovic@sydney.edu.au

Components: 6,820 words, 12 figures, 3 tables, Supplementary Material

Keywords:

Index terms:

Abstract

The Eocene India-Eurasia collision is a first order tectonic event whose nature and chronology remains controversial. We test two end-member collision scenarios using coupled global plate motion-subduction models. The first, conventional model, invokes a continental collision soon after ~60 Ma between a maximum extent Greater India and an Andean-style Eurasian margin. The alternative scenario involves a collision between a minimum extent Greater India and a NeoTethyan back-arc at ~60 Ma that is subsequently subducted along southern Lhasa at an Andean-style margin, culminating with continent-continent contact at ~40 Ma. Our numerical models suggest the conventional scenario does not adequately reproduce mantle structure related to Tethyan convergence. The alternative scenario better reproduces the discrete slab volumes and their lateral and vertical distribution in the mantle, and is also supported by the distribution of ophiolites indicative of Tethyan intra-oceanic subduction, magmatic gaps along southern Lhasa and a two-stage slowdown of India. Our models show a strong component of southward mantle return flow for the Tethyan region, suggesting that the common assumption of near-vertical slab sinking is an oversimplification with significant consequences for interpretations of seismic tomography in the context of subduction reference frames.

1. Introduction

The closure of the Tethyan ocean basins was responsible for the uplift of the vast Alpine-Himalayan orogenic belt stretching from central Europe to Southeast Asia [*Acharyya*, 1998; *Golonka*, 2004; *Stampfli and Borel*, 2002], with significant consequences for regional tectonics and global climate [*Raymo and Ruddiman*, 1992; *Tapponnier et al.*, 1982]. The final stage of Tethyan evolution involved the separation of India from Gondwana sometime after ~130 Ma [*Robb et al.*, 2005], marked by magnetic anomaly M10 offshore Western Australia, to open the Indian Ocean at the expense of the intermediary Meso- and Neo- Tethys [*Veevers et al.*, 1991]. The Yarlung-Tsangpo Suture Zone (Figure 1) represents the main contact between the Indian and Eurasian continents where Indian epicontinental shallow-marine sediments juxtapose those of Eurasian affinities [*Najman and Garzanti*, 2000; *Searle et al.*, 1987; *Yin and Harrison*, 2000]. However, the timing of the first mixing between Greater Indian and Eurasian sediments remains controversial, resulting in poorly constrained dynamics of the collision. We aim to use numerical models and evidence from the subsurface to help constrain the nature and chronology of the India-Eurasia collision. A better understanding of the convergence history has the potential to increase our understanding of the timing of uplift in proximal orogenic belts, regional volcanic activity, denudation histories and deformation.

The established view of the collision is based on interpretations of magnetic lineations in the Indian Ocean seafloor that are used to derive India-Eurasia convergence histories [*Lee and Lawver*, 1995; *van Hinsbergen et al.*, 2011a]. Conventional interpretations link the reduction in India-Eurasia convergence rates and the first influx of India-derived sediments at the Eurasian margin to continent-continent collision sometime between ~65 and 50 Ma [*Garzanti*, 2008; *Lee and Lawver*, 1995; *Patriat and Achache*, 1984; *Replumaz and Tapponnier*, 2003; *Rowley*, 1996; *Searle et al.*, 1987]. We define “conventional models” as those that have long-lived Andean subduction along southern Lhasa, with a terminal collision between the two continents occurring at the first significant slowdown of India-Eurasia convergence. An example of such models is one proposed by *Lee and Lawver* [1995], which implies collision between a very large Greater India and southward displaced Lhasa at ~55 Ma, forming the inspiration for one end-member scenario in our numerical models. Alternative models now place the continental collision as late as 34 Ma [*Aitchison et al.*, 2007]. Such models link the first slowdown in India-Eurasia convergence after 60 Ma to an initial collision with a NeoTethyan intra-oceanic island-arc, followed by continent-continent collision closer to ~40 Ma [*Aitchison et al.*, 2007; *Davis et al.*, 2002; *Hafkenscheid et al.*, 2006; *Klootwijk et al.*, 1985; *Van der Voo et al.*, 1999b]. We test two end-member plate kinematic scenarios of the India-Eurasia collision to identify whether long-lived Andean style subduction at the Eurasian margin implied by conventional models can account for the subducted slabs observed in seismic tomography of the mantle, or whether a Meso- and Neo-Tethyan back-arc basin, proposed in alternative models, is necessary to reproduce the present-day mantle structure. The kinematic scenario that better reproduces the large latitudinal range of slab material at mid-mantle depths interpreted from mantle tomography would therefore better represent the nature and chronology of the India-Eurasia collision.

1.1. Rotation models of India-Eurasia convergence

The convergence history quoted by most authors to infer initial continental collision is usually based on a single plate motion model, with specific plate circuits and inherent interpretive biases in identifying magnetic lineations. Therefore, it is important to identify whether the choice of rotation models alone can account for the wide range in collision timing interpretation. Multiple plate kinematic models exist that document the relative motion between India and Eurasia, including those of *Lee and Lawver* [1995], *Müller et al.* [2008], *Molnar and Stock* [2009], and Model A of *van Hinsbergen et al.* [2011a]. When comparing the convergence rates of India to Eurasia across published models (Appendix A and B), standardised to the geological time-scale of *Cande and Kent* [1995], it is evident that the convergence-rate drops, and therefore inferences of initial collisions, are entirely model-dependent and do not occur during the same time intervals with different rotation models (Figure 2). The *Lee and Lawver* [1995] and *Molnar and Stock* [2009] rotation models imply a convergence rate drop to less than 12 cm/yr at ~56 Ma, followed by other stepwise decreases in convergence velocities at ~47 Ma and ~40 Ma, while the initial convergence velocity decrease to values below 12 cm/yr occurs at ~55 Ma in *Müller et al.* [2008], and ~51 Ma in *van Hinsbergen et al.* [2011a]. All of the rotation models suggest multiple stepwise decreases in India-Eurasia convergence, and therefore it is difficult to identify a singular event related to India-Eurasia continental collision. The initial slowdown in seafloor spreading at ~52 Ma on the Central and Southeast Indian ridges, interpreted by *Cande et al.* [2010] using updated seafloor spreading data and plate circuits, highlights that the choice of plate circuits and the identification of magnetic lineations can significantly change plate velocity trends, meaning that conclusions based on convergence rate trends alone should not be used to infer collision timing.

1.2. Pre-collision margins

Much of the collision timing controversy stems from the poor constraints on the pre-collision margins of both Eurasia and Greater India [*Aitchison et al.*, 2007; *Hafkenscheid et al.*, 2006]. The northward extent of Greater India in the *Lee and Lawver* [1995] model is derived from the reconstructed position of India and Eurasia at ~55 Ma, at which time the gap between the two continents is filled to ensure contact between Lhasa and India. However, this assumes that the ~55 Ma event, marked by a drop in the convergence rate in their rotation model, is a continent-continent collision, and that the active pre-collision Eurasian margin was an Andean-style margin along southern Lhasa. In addition, microcontinent formation, whereby a passive continental margin is rifted along a preferential landward detachment zone, would have successively removed continental blocks from the Tethyan Gondwana margin [*Müller et al.*, 2001] to reduce the size of Greater India. Retro-deformation of the crumpled and under-thrust Indian crust below Tibet suggests that the maximum northward extent of the passive Indian continental margin was no more than 950 km of the present-day suture zone [*Replumaz and Tapponnier*, 2003], which agrees with the proposed smaller extent bound by the Wallaby-Zenith Fracture Zone at pre-breakup fit [*Ali and Aitchison*, 2005] (Figure 4). A smaller Greater India is also compatible with the tomographically-derived pre-collision margin of Greater India of *Replumaz et al.* [2010] and the correlations of a steeply-dipping unbroken slab in the upper mantle near the Yarlung-Tsangpo Suture Zone to the subducted continental lithosphere of Greater India by *Van der Voo et al.* [1999b]. A range of geometries have been proposed for this passive margin and are discussed at length in *Klootwijk and Conaghan* [1979] and *Ali and Aitchison* [2005].

In addition to the uncertain size of Greater India, the pre-collision margin of Eurasia is poorly understood. New paleomagnetic data, corrected for sediment compaction and inclination shallowing [*Tan et al.*, 2010], suggest that models such as *Lee and Lawver* [1995] place the Lhasa terrane, forming the active pre-collision margin, up to ~10° too far south, indicating that early contact at ~55 Ma between a maximum extent Greater India and southward-displaced Lhasa may be problematic. Paleomagnetic studies which show an initial overlap between apparent polar wander paths of India with respect to Asia suggest contact at 46 ± 8 Ma [*Dupont-Nivet et al.*, 2010] or as late as ~43 Ma [*Tan et al.*, 2010], indicating that collision timing derived from paleomagnetic data has large inherent uncertainties and cannot be used alone to define the initial timing of continent-continent collision. Reconstructing the geometry of Greater India and Lhasa as proposed by *Lee and Lawver* [1995] shows that initial contact occurs between 54 and 49 Ma across the five different rotation models (Table 1 highlighted column and Figure 3), which highlights the model-dependence of interpretations based on rotation models to infer collision timing (Figure 2). When reconstructing the maximum extent of Greater India from *Lee and Lawver* [1995] and a range of proposed paleomargins of Eurasia, the effect on the collision timing is much more pronounced than varying the rotation model alone, resulting in a collision window of 15 Myr (Figure 3, Table 1). Thus the choice of pre-collision margins of both India and Eurasia is the dominant variable determining the timing of continental contact in plate reconstructions.

Independent of the rotation models and inferences of pre-collision margins, stratigraphic studies focused on the horizons that mark the first input of Tethyan sediments overlying sediments of Eurasian affinities to date the onset of continent-continent collision older than ~50 Ma [*Clift et al.*, 2002]. However, a re-interpretation of this horizon by *Henderson et al.* [2011] shows only a break in Eurasian sedimentation, with India-derived sediments occurring higher in the sedimentary column, indicating that continental collision may have occurred later than the ~50 Ma age proposed by *Clift et al.* [2002]. Recent studies of sedimentary sequences and ophiolite belts near the main suture zone suggest a well-established intra-oceanic subduction system in the NeoTethys whose closure preceded the main continent-continent collision [*Aitchison et al.*, 2007; *Aitchison et al.*, 2000; *Davis et al.*, 2002; *McDermid et al.*, 2002; *Ziabrev et al.*, 2004]. Ophiolites of remnant back-arcs in the western NeoTethys have been studied extensively, including the Semail supra-subduction zone ophiolite that was emplaced after 90 Ma, and it has been suggested that a similar scenario existed in the central NeoTethys [*Hafkenscheid et al.*, 2006; *Pearce et al.*, 1981; *Shervais*, 2001; *Stampfli and Borel*, 2002]. Cessation of arc-magmatism along the Kohistan-Ladakh arc at ~61 Ma can be interpreted as the onset of ophiolite emplacement onto Greater India [*Khan et al.*, 2009], while further east the Zedong Ophiolite was likely to have been emplaced at ~57 Ma [*Ali and Aitchison*, 2008]. The precise dating of ophiolite emplacement onto Greater India is controversial because it relies on dating the first appearance of serpentinite-rich ophiolitic sediment or paleobiological methods. It is also difficult to constrain the southward extent of the proposed intra-oceanic magmatic arc using paleomagnetic data, with inherent shortcomings and typical latitudinal error margins of ± 5° for the region [*Sun et al.*, 2010] that are as large as the proposed back-arc basin itself.

1.3. Seismic tomography and numerical models of the collision

In light of the complex geology, some authors have looked to the sub-surface for independent clues of Tethyan subduction histories. The distribution of positive seismic velocity anomalies identified in P-wave seismic mantle tomography north of the equator and beneath the collision zone have been linked to long-lived Tethyan subduction evolution [*Hafkenscheid et al.*, 2006; *Van der Voo et al.*, 1999b]. *Van der Voo et al.* [1999b] link the latitudinal distribution of discrete slabs in the lower mantle to paleo-subduction zone locations, and suggest that a subducted NeoTethyan back-arc basin better accounts for the lateral and vertical distribution of slab material. The existence of an intra-oceanic subduction system would have increased the southward extent of the Eurasian active margin. Consequently, the subducted NeoTethyan slab should be found south of the present-day Yarlung-Tsangpo Suture Zone [*Hafkenscheid et al.*, 2006] assuming little lateral migration of slabs following subduction, following *Van der Meer et al.* [2010], and the temporal persistence of slab-derived thermal anomalies in the mantle [*Jarvis and Lowman*, 2005; *Van der Voo et al.*, 1999a].

The quantitative analysis by *Hafkenscheid et al.* [2006] compared expected Tethyan slab volumes from plate reconstructions with positive seismic velocity anomalies of 0.2% and higher from the P-wave tomography model of *Bijwaard et al.* [1998], indicating that long-lived NeoTethyan subduction along an Andean-style margin does not adequately account for the present-day mantle structure. Their scenario of intra-oceanic subduction along a large back-arc basin better reproduces the volume and distribution of positive seismic velocity anomalies in the mantle. In their model India collides with an intra-oceanic island arc at ~65 Ma and Andean-style subduction is subsequently initiated along continental Eurasia to consume the back-arc basin by ~48 Ma

[*Hafkenscheid et al.*, 2006]. *Jarvis and Lowman* [2005] tested the viability of such subduction scenarios using 2D numerical subduction models of the India-Eurasia collision, identifying the need to independently reproduce and quantify the observed Tethyan mantle seismic velocity anomalies using numerical subduction models.

2. Method

2.1. Kinematics of the India-Eurasia collision

Our global plate kinematics are based on the tectonic model of *Müller et al.* [2008] and *Seton et al.* [submitted] and were used to generate the seafloor age-grids and plate velocities in 1 Myr intervals (Figure 5). Intersecting plate boundaries through time were implemented in *GPlates* (www.gplates.org) to define continuously closing plate polygons that cover the entire globe, modified from *Gurnis et al.* [2012]. We use a moving hotspot absolute reference frame from 100 Ma [*O'Neill et al.*, 2005] and true-polar wander-corrected motions of Africa form 100 to 200 Ma [*Steinberger and Torsvik*, 2008] in order to isolate the plate-mantle system. The fixed hotspot absolute reference frame of *Müller et al.* [1993] was also considered, but the limited temporal span of ~130 Myr made it unsuitable for our global models. In addition, the *Van der Meer et al. [2010]* subduction reference frame was not used as it would result in circular reasoning while imposing the assumption of vertical sinking of all slabs with a constant sinking rate. When extending the finite rotations of the fixed hotspot reference frame (FHS) to 200 Ma, the reconstructed paleo-margin of Eurasia is offset ~10° northward at 200 and 150 Ma when compared to the moving hotspot and true-polar wander corrected frame of reference in our global models (Figure 6). The subduction reference frame results in a longitudinal offset of the paleo-margin at these times due to the inherent longitudinal correction in this reference frame. At 100 and 50 Ma all reference frames produce a similar paleo-reconstruction of the Tethyan and Pacific active margins, with differences that we assume are not significant enough to be detectable in seismic tomography.

A scenario broadly similar to that of *Lee and Lawver* [1995] with a large Greater India and long-lived Andean-style subduction in the NeoTethys at the continental margin was implemented as the conventional model. The southward extent of undeformed Eurasia was based on the geometry proposed by *Replumaz et al.* [2004] and the pre-collision southward extent of Lhasa based on *Lee and Lawver* [1995] (Figure 5, left column). The size of Greater India and the NeoTethyan intra-oceanic subduction of the alternative kinematic scenario are largely based on the preferred subduction model of *Hafkenscheid et al.* [2006], and a scenario slightly modified from that proposed by *Ziabrev et al.* [2004], *Ali and Aitchison* [2008] and *Aitchison et al.* [2011] (Figure 5, right column). The rotations of India and Eurasia were not modified, and only the pre-collision margins were varied. The smaller Greater India is based on the interpretations of *Replumaz et al.* [2010] and *Ali and Aitchison* [2005] (Figure 4).

2.2. Back-arc extent from age-coded slabs in seismic tomography

The extent of the proposed NeoTethyan intra-oceanic subduction zone in the alternative scenario was constructed by determining the approximate location of paleo-subduction using age-coded depth slices of subducted material in P- and S- wave seismic tomography models (Figure 7, Appendix C). We interpret positive seismic velocity anomalies in the mantle that correlate across both P- and S- wave tomography models to be slab remnants representing thermally-perturbed mantle [*Becker and Boschi*, 2002]. Following *Hafkenscheid et al.* [2006], we assumed an average sinking rate of 3 cm/yr in the upper mantle for the Tethyan subduction system. For the lower mantle, we assumed a sinking velocity of 1.2 cm/yr from the global tomography interpretations of *Van der Meer et al.* [2010]. We assume purely vertical sinking of slabs in the mantle for this workflow, and we use our geodynamic models to determine the plausibility of such assumptions. In the 1604 km depth slice from the *Li et al.* [2008] P-wave model (MIT-P), slab material which corresponds to ~100 Ma with the assumed sinking velocities, shows a large mismatch of up to ~20° latitude between the *Replumaz et al.* [2004] Eurasian continental margin and the slab material in the depth slice (Figure 7). The 1658 km depth slice in the *Grand* [2002] S-wave model (GRAND-S), corresponding to ~105 Ma, shows a similar mismatch. We used the southern boundary of the positive seismic velocity anomaly as the maximum southward extent of the NeoTethyan back-arc basin. We then created rotations and isochrons to simulate the opening of a back-arc basin and to generate seafloor age-grids consistent with the alternative scenario. As the Lhasa terrane accreted onto Eurasia at the Jurassic-Cretaceous boundary [*Golonka*, 2004], we assumed that NeoTethyan back-arc basin opening occurred between 150 and 120 Ma with a full spreading rate of about 5.5 cm/yr and a maximum north-south extent of 1600 km. The back-arc closes only following collision with the Greater Indian margin at about 60 Ma, with back-arc subduction and continental suturing occurring by ~40 Ma. Although a mechanism for initiating intra-oceanic subduction in the Tethys is enigmatic, we assume that the intra-oceanic subduction system could develop from possible MesoTethyan slab rollback, back-arc rifting and spreading following the welding of the Cimmerian terranes onto southern Eurasia in the late Jurassic.

2.3. Global subduction model setup

As plate motions are the surface manifestation of mantle convection [*Bercovici et al.*, 2000], forward numerical models that couple plate velocities with subduction allow us to predict present-day mantle structure that can be validated using seismic tomography [*Ricard et al.*, 1993]. We used a modified version of the finite element code *CitcomS* [*Tan et al.*, 2006; *Zhong et al.*, 2000] to solve for thermal convection within an incompressible viscous mantle with plate velocities applied as kinematic boundary conditions on the upper surface. The subduction models used a mesh with lateral grid spacing of 50 and 23 km on the surface and at the core-mantle boundary (CMB) respectively (Table 2). To balance the reduced resolution closer to the surface, we refined the vertical resolution of the mesh in the upper mantle and used a global domain to avoid edge effects that would normally occur in regional models. A half-space cooling model for the oceanic lithosphere was progressively assimilated into the numerical models, following *Matthews et al.* [2011], using the seafloor age-grid from our plate reconstructions. The continental lithosphere is divided into three categories: Archean, Proterozoic and Phanerozoic [*Artemieva*, 2006] for which we impose a thermal lithosphere thickness of 215, 165 and 100 km respectively [*Artemieva*, 2009]. The thermal structure of slabs is imposed at each timestep with assimilation stencils that extend to a distance of 350 km around a subduction zone, and a 200 km curvature radius of subducting slab material (Gurnis, in prep.). We use the parameters in Table 3 to define our Rayleigh number for mantle depths, $Ra = \sim 4 \times 10^7$, and we apply temperature-dependent viscosity following

$$\eta = \eta_0 \times \exp\left(\frac{E_\eta}{T^* + T_\eta} - \frac{E_\eta}{0.5 + T_\eta}\right),$$

where η_0 is the reference viscosity, E_η is the activation energy, $T^* = \min(\max(T, T_{min}), T_{max})$, with T *as* the temperature, T_{min} and T_{max} the minimum and maximum temperatures of the mantle, respectively, and T_η the activation temperature (Figure 8, Table 3). We ignore the effects of internal heating from radioactive decay, but allow the bottom thermal boundary layer to develop dynamically through basal heating with a CMB non-dimensional temperature of 1. A viscosity contrast of 100 between the upper and lower mantle was implemented in our model runs that is consistent with the findings of *Alpert et al.* [2010] and *Jarvis and Lowman* [2005; 2007].

2.4 Comparison to seismic tomography

A number of mantle seismic tomographic models were chosen to compare with the predictions of the numerical models. As each seismic tomography model has inherent assumptions, variable coverage, vertical and lateral resolutions, and damping parameters [*Grand*, 2002; *Romanowicz*, 2008], we consulted a number of models. Although P-wave models tend to have higher resolutions and better-resolved subduction zones, coverage for oceanic regions is limited [*Grand*, 2002]. Longer wavelength features in the mantle are better imaged with S-wave models, which also tend to have better coverage in the southern hemisphere and in the Pacific [*Romanowicz*, 2008]. We do not attempt to analyse the mantle structure below 2500 km depth which likely has significant chemical heterogeneities [*Masters et al.*, 2000], and as both kinematic scenarios invoke subduction in the northern hemisphere, we avoided analysing southern hemisphere mantle structure due to lower resolution seismic tomographic models. A description of all tomographic models used can be found in Appendix D.

3. Results

3.1. Vertical subduction zone evolution

A vertical slice along a great circle segment between 10°S, 55°E and 45°N, 90°E was chosen for comparison between the conventional and alternative scenario as it was the most representative of the NeoTethyan convergence and proposed back-arc evolution. Plate kinematics between 200 and 150 Ma are common to both scenarios (Figure 9a), with continuous Andean-style subduction along the Eurasian margin. The subduction zone retreats almost 10° to the south between 200 and 150 Ma due to the clockwise rotation of Eurasia and the accretion of Cimmerian terranes to close the PaleoTethys. The vertical sinking velocity of slabs average ~1.6 cm/yr in the mid-mantle between 200 and 170 Ma for the Tethyan subduction system, with sinking rates as low as ~1.3 cm/yr in the lowermost mantle between 170 and 150 Ma. We do not estimate upper mantle sinking velocities from our models since slabs are imposed to a depth of 350 km. About 5° of southward advection of the unbroken PaleoTethyan slab occurs between 170 and 150 Ma, after which the kinematic boundary conditions on the surface begin to diverge between the conventional and alternative scenarios.

The conventional scenario has continued Andean-style subduction (Figure 9b), while a large back-arc opens in the alternative scenario to shift subduction in the central MesoTethys to ~15°N by 120 Ma (Figure 9c). A slab window forms between 150 and 120 Ma in both scenarios due to the intersection of the MesoTethyan mid-ocean ridge and the subduction zone [*Thorkelson*, 1995]. The continuous older Paleo- and Meso- Tethyan slab approaches the CMB, while the subduction of the leading edge of the younger slab is deflected at the transition zone in both scenarios. The younger slab drapes across the transition zone between ~15 and 25°N in the alternative scenario as the subduction zone migrates southward during back-arc opening between 150 and 120 Ma. By 90 Ma, the slab in the conventional model has penetrated the transition zone and is sinking at latitudes of ~25 to 30°N, while the upper mantle slab in the alternative model is only starting to penetrate the 660 km transition. The lower mantle slab in both models has already started to drape over the CMB, with considerable southward displacement by 90 Ma. Importantly, subduction is occurring at ~15°N in the alternative model by 90 Ma, rather than ~25°N in the Andean-style subduction of the conventional model. The lowermost mantle structure is similar in both models by 60 Ma, while mid- and upper- mantle structure differs considerably in the alternative scenario by 55 Ma due to the initial collision between Greater India and the NeoTethyan island arc. This initial collision causes NeoTethyan slab break-off and initiates the subduction of the back-arc along southern continental Lhasa. Final slab break-off occurs after ~55 Ma in the conventional model following the onset of continental collision and suturing between Greater India and continental Eurasia. The back-arc slab detaches by ~40 Ma in the alternative scenario due to the later continental collision between Eurasia and a smaller Greater India. Two discrete slab volumes are sinking at mid-mantle depths by 30 Ma in the alternative scenario, in contrast to the single descending slab at similar depths in the conventional model. Slab material sourced from the Pacific north of ~35°N at depths greater than ~1200 km appears by 30 Ma and interacts with the Tethyan slabs in the lowermost mantle.

The present-day prediction of mantle structure from both scenarios (Figure 10a) was compared to equivalent vertical slices in a range of mantle tomographic models (Figure 10b, Appendix E). P- and S- wave models, suggest the distribution of Tethyan slabs range from near-equatorial latitudes, to as far north as 35°N – with a wide band of coherent positive seismic velocity anomalies at mid mantle depths between ~800 and 2400 km. The numerical model of the conventional scenario predicts a single slab at mid-mantle depths (~1200 to 2000 km) with a latitudinal range of ~15 to 25°N, while the alternative scenario predicts two discrete mid-mantle slabs. The back-arc slab is found at latitudes between 20 and 25°N at mid-mantle depths, merging with the Paleo- and Meso-

Tethyan slabs in the lower mantle, while the youngest NeoTethyan slab is found at depths between ~1000 and 1300 km between ~0 and 15°N. Thus the two numerical model predictions vary the most between ~1000 and 1300 km depth. The mid-mantle slabs that are common to both scenarios at present-day can be accounted for in all seismic tomographic models, albeit the corresponding seismic velocity anomalies are more smeared than the thermal anomaly predicted by the numerical models. All seismic tomography models suggest the existence of a discrete slab, offset further south of the main slab volume observed at mid-mantle depths. The latitudinal offset varies in the tomographic models, with GRAND-S suggesting a small slab between ~10-15°N at ~1500 km depth, while other P- and S- wave models suggest a shallower depth of ~1000 km for this seismic velocity anomaly between ~5°S and 15°N. The conventional scenario does not reproduce the large latitudinal range of slab material in the mid-mantle, while the alternative scenario produces a better match to observations of present-day mantle structure. The continuity of an upper mantle slab with the remaining mid-mantle slab material is questionable as GyPSuM-P and SB4L18 suggest no link across the transition zone, while the remaining tomographic models support this link that is not replicated in either numerical models of Tethyan convergence.

3.2. Lateral distribution of slab material and lateral mantle flow

The horizontal depth slices of seismic tomography from a number of models between ~1000 and 1300 km depth highlights the differences between the conventional and alternative subduction scenarios with a large latitudinal range of positive seismic velocity anomalies (Figure 11, Appendix F). At a depth of ~1000 km, the S-wave tomographic models (SAW24B16 and GRAND-S) support the existence of slab material further south than can be accounted for by the conventional model (red contour). Although the P-wave MIT-P model also suggests a larger latitudinal range of slab material at this depth, the amplitude of the positive seismic velocity anomaly is diminished in oceanic regions, an expected artefact of most P-wave models. At a depth of ~1250 km, the discontinuity of the main northern slab is better reproduced by the alternative scenario, while both numerical models provide a good match in the Java-Sunda region. The GRAND-S model does suggest the existence of a discrete slab south of the main seismic velocity anomaly, but it is further east than predicted by the alternative subduction scenario. The positive seismic velocity anomalies at this depth extend to equatorial latitudes, which cannot be explained by the conventional scenario of subduction. The match between the southernmost slab predicted by the alternative model at a depth of ~1300 km is highest with SAW24B16 and GyPSuM-P. The amplitude of the corresponding positive seismic velocity anomaly in the MIT-P model is diminished, and may be due to the inherent shortcoming of some P-wave models where the amplitude of seismic velocity anomalies diminishes significantly away from continental regions with high seismic ray coverage. The continuity of the main northern slab volume is also unclear at this depth, with SAW24B16 and MIT-P suggesting a discontinuous slab while GyPSuM-P indicates slab continuity. The 1445 km depth slice in GRAND-S shows a large discrete slab south of the main slab volume, but is not reproduced by either the conventional or alternative scenario. This is largely due to the smearing effect in tomographic models, contrasting the well-defined slab contours of thermal anomalies from numerical models.

The southward extent of our back arc in the alternative scenario was guided by seismic tomography images with the initial assumption of vertical sinking of slab material through the mantle. However, our global flow models show that slabs are advected by lateral return flow at mid-mantle depths, with significant variations in the mantle flow direction and magnitude through time (Figure 12, Appendix G). Our plate motions contain a net rotation component [*Torsvik et al.,* 2010] that induces shear deformation distributed through the mantle. It is beyond the scope of this study to carry out a global analysis of net mantle rotation versus regional lateral mantle flow. For this reason, we limit our analysis of regional lateral mantle flow to its north-south component (red arrows in Figure 12) that is unaffected by longitudinal net rotation (which represents the bulk net rotation in our model).

Our results show that the northward subduction of Tethyan slabs leads to a significant southward return flow at mid-mantle depth. A strong southward component of flow dominates at 90 Ma at a depth of ~1000 km, where NeoTethyan slabs are strongly advected. However, the southward component of flow wanes between 60 and 30 Ma, and returns to a strong southward-directed advective flow towards the present-day. The advection of slabs reveals that the assumption of vertically sinking slabs used to build a subduction reference-frame [*Van Der Meer et al.*, 2010] is an over-simplification. To the same effect, we also note that the constant sinking rate 1.2 cm/yr in the lower mantle assumed in our initial slab age-coding workflow is slightly smaller than the 1.3 to 1.6 cm/yr range evident for the Tethyan region in the numerical models.

4. Discussion

4.1. Insights from numerical models

Interpretation of slab material in our subduction models relies on the first-order comparisons between thermal heterogeneities and seismic velocity anomalies, assuming that high seismic velocity anomalies that correlate across P- and S- wave mantle seismic tomography are colder, denser and therefore represent sinking materials from subduction zones [*Simmons et al.*, 2009]. Although the viscosity contrast between the upper and lower mantle is not well constrained, our results show that a viscosity contrast of 100 between the upper and lower mantle is sufficient to retain coherent Meso- and Neo- Tethyan slabs at mid-mantle depths that match the observed mantle structure from seismic tomographic models and are consistent with previous studies [*Hager*, 1984; *Jarvis and Lowman*, 2005]. Our global subduction models show that the conventional scenario of long-lived Andean subduction along continental Eurasia does not reproduce the latitudinal range of slab material at mid-mantle depths at present day. Our models also show that the subduction of additional oceanic lithosphere, such as a large back-arc basin, is necessary to account for the present-day mantle structure, and that the overall chronology likely involved initial contact between Greater India and an intra-oceanic island arc.

The alternative scenario in our study reproduces discrete parallel slab volumes at mid-mantle depths, largely consistent with interpretations of *Hafkenscheid et al.* [2006] and *Van der Voo et al.* [1999b]. While most seismic tomography models at depths of ~1000 to 1300 km suggest a southwardly-offset slab, the longitudinal position of this volume varies somewhat across the tomographic models. Although our numerical models predict a significant westward mantle flow at mid-mantle depths (Figure 12, Appendix G), we do not interpret this observation, as our imposed plate kinematics imply a ~0.12°/Myr westward net rotation of the lithosphere as described by

Torsvik et al. [2010] and therefore it is difficult to isolate the local east-west component of flow from the effects of global lithospheric net rotation. Independent of longitudinal flow, our models suggest a southward flow of Tethyan slab material in the mantle that we interpret as return flow from north-directed subduction. Therefore, we suggest that while it is useful to the first order, the assumption of vertically sinking slabs and constant sinking rates [*Van Der Meer et al.*, 2010] is an oversimplification of complex mantle flow. An improvement to our method of age-coding slabs in tomography would be to backward-advect slabs from seismic tomography using an adjoint convection model in order to correct for lateral mantle flow as demonstrated by *Liu and Gurnis* [2008].

The longitudinal location of the back-arc slab may also vary if we take into account the evolution of the Western and Easternmost Tethys, which was beyond the scope of this study. The motion of Argoland (West Burma Block) in our models, as a Gondwana-derived terrane that accreted onto Eurasia at ~80 Ma [*Heine and Müller*, 2005], may have closed a back-arc that extended along the entire Eurasian margin as in the model proposed by *Stampfli and Borel* [2002]. In addition, there may have been one or more episodes of back-arc opening in the Tethys as observed in the western Pacific [*Clark et al.*, 2008]. In our alternative scenario we implement a long-lived Tethyan back-arc that is in some ways similar to the Kohistan-Ladakh back-arc system, thought to have opened at 134 ± 3 Ma based on K-Ar ages and closed well before the India-Eurasia collision [*Allegre et al.*, 1984; *Khan et al.*, 2007; *Pudsey*, 1986]. However, some authors have suggested that India first collided with the Kohistan-Ladakh magmatic arc by 55 Ma [*Gaetani and Garzanti*, 1991; *Khan et al.*, 2009]. Earlier studies, such as *Dewey et al.* [1988], had also suggested a late continental collision at ~45 Ma, with a Cretaceous-age emplacement of the Spongtang Ophiolite (Figure 1). However, there is little evidence that the Kohistan-Ladakh or the Spongtang arc system extended eastward along the Indus-Tsangpo suture as in our alternative scenario. If the initial slowdown of India at ~55 Ma was unrelated to collision with an island arc, then the subduction of a large buoyant structure on the downgoing plate, such as an oceanic plateau or seamount chain, may have impeded subduction and caused a slowdown in convergence. However, we predict that such a scenario would not result in a large latitudinal range of slab material as observed in mantle tomography. Apart from the subduction of a back-arc basin, it is also possible to subduct additional oceanic material along southern Eurasia if a microcontinent had rifted off Greater India to create a seaway as proposed by *Roy* [1976]. However, little trace of such features exists in the suture zone and so they were either completely subducted, not yet mapped in the remote regions of the collision zone or they did not exist.

In addition to the possibility of intra-oceanic subduction significantly altering the dynamics of India-Eurasia convergence, mantle plumes have recently been implicated in accelerating India's advance toward Eurasia prior to collision [*Cande and Stegman*, 2011; *van Hinsbergen et al.*, 2011a]. *Cande and Stegman* [2011] associate the acceleration of India at the onset of Anomaly 30 (~67 Ma) with the arrival of the Reunion plume head at the India-Africa ridge and to the emplacement of the voluminous Deccan Traps on the Indian continent. They find that the motion of India slows considerably by 52 Ma, followed by a more significant decrease in speed after 45 Ma accompanied by a change in spreading direction between India and Africa. A scenario with initial collision at ~52 Ma would require a smaller back-arc basin than we implemented or a smaller Greater India, leading to a later initial collision and possible continental contact at ~45 Ma. This is plausible as both the extent of Greater India and the proposed NeoTethyan back-arc basin are uncertain.

4.2. Insights from surface geology

The large back-arc basin of the alternative scenario better fits observations of subducted slab material in mantle tomography to suggests that pre-Eocene subduction occurred at least 10º further south than can be explained by subduction at an Andean-style margin proposed by conventional models. To produce Andean-style subduction this far south would imply that either Lhasa was much further south at this time or that the entire Asian continent was decoupled from European continent. However, the potential regions of decoupling between Europe and Asia, notably the Ural mountains, have been discounted as the source for the large-scale independent motion of Asia relative to Europe in the Cenozoic [*Lippert et al.*, 2011]. A recent review of paleomagnetic data from the volcanic Linzizong Group by *Yi et al.* [2011] suggests that Lhasa was at a latitude of 6.1 ± 8.5°N (64-60 Ma), 12.9 ± 4.6°N (60-50 Ma) and 19.3 ± 4.7°N (50-44 Ma) in the early Cenozoic. The study by *Sun et al.* [2012] indicates that the Lhasa terrane was at 15.2 ± 6.3°N at collision timing of ~54-47 Ma derived from the overlap of Tethyan Himalaya apparent polar wander paths with those of Lhasa. Others report that the paleolatitude of the Lhasa terrane was not further south than 20°N throughout Eocene time based on paleomagnetism of Paleogene volcanics [*Lippert et al.*, 2011]. Unfortunately, paleomagnetic data alone places Lhasa anywhere between being south of the equator or in excess of 20°N in pre-collision times. However, equatorial or low latitude positions of Lhasa in the early Eocene would imply extreme post-collisional north-south shortening of the terrane, where only ~290 km north-south shortening of the terrane is recorded in the geology from ~100 to 20 Ma [*van Hinsbergen et al.*, 2011b].

In the region of Mt Everest, an initial high pressure and temperature metamorphic event at ~39 Ma [*Cottle et al.*, 2009] may be indicative of continent-continent collision between Greater India and Lhasa. This would explain a further significant drop in India-Eurasia convergence rates by ~40 Ma (Figure 2). Additionally, studies of sediments near Mt Everest indicate a marine depositional setting prevailing as late as 34 Ma [*Wang et al.*, 2002], suggesting that suturing was likely diachronous along the margin and that final collision between India and Eurasia occurred much later than India's initial slowdown. Reactivation of the major Altyn Tagh fault by 40 Ma [*Liu et al.*, 2007], strike-slip motion along the Ailao Shan-Red River shear zone by 35 Ma [*Leloup et al.*, 2007; *Leloup et al.*, 2001] and post-collisional deformation propagating north with shortening and exhumation propagating north in the Tian Shan at ~25 Ma [*Dumitru et al.*, 2001] suggest an early Paleogene continent-continent collision would require a ~20 Myr time lag in regional geological responses. The absence of volcanic activity along southern Lhasa, at least in the late Cretaceous [*Chung et al.*, 2005], also casts doubt on continuous Andean-style subduction in the NeoTethys. However, the first pulse of Transhimalayan Batholith emplacement at ~100 Ma [*Debon et al.*, 1986; *Miller et al.*, 1999] is incompatible with our alternative scenario, and may suggest short-lived pulses back-arc seafloor subduction. The Linzizong Volcanics (Figure 1), previously interpreted as Andean-style subduction-related suites, along with another pulse of Transhimalayan Batholith emplacement [*Debon et al.*, 1986; *Miller et al.*, 1999], between ~65 and 40 Ma [*Xia et al.*, 2011] are observations that are compatible with the closure of a back-arc basin in our alternative scenario. Similarly, the generalized stratigraphic interpretations of *Aitchison et al.* [2011] indicate a hiatus in pluton emplacement from ~80 to 65 Ma. However, the duration of that magmatic gap depends on how well temporally- and spatially- sampled the magmatic suites are in the collision zone. We speculate that the Linzizong Volcanics are emplaced as a result of Andean-style subduction of the NeoTethyan back-arc between ~65 and 40 Ma, after which continental deformation and extrusion dominated.

5. Conclusion

Our study demonstrates that competing end-member kinematic scenarios of plate convergence can be tested using global subduction models whose predictions can be validated using both surface geology and sub-surface mantle structure. Numerical models of NeoTethyan intra-oceanic subduction better reproduce the volumetric, vertical and lateral distribution of slab material interpreted from P- and S- wave mantle tomography models than long-lived Andean subduction along southern Lhasa. In this way we are able to show that the NeoTethys was likely consumed along an intra-oceanic island arc that was accreted to the leading margin of Greater India during the initial convergence rate drop with Eurasia at ~60 Ma. The subduction of additional oceanic crust from a Cretaceous-age back-arc along southern Lhasa is also largely consistent with the timing of magmatic episodes north of the Yarlung-Tsangpo Suture Zone and the large latitudinal range of positive seismic velocity anomalies in seismic tomography beneath the convergence zone. The significant convergence rate drop between India and Eurasia by ~40 Ma correlates to the final continent-continent collision that better explains changes in magmatism [*Debon et al.*, 1986; *Miller et al.*, 1999; *Xia et al.*, 2011], high pressure/temperature metamorphism near the suture zone [*Cottle et al.*, 2009], marine deposition as young as ~34 Ma [*Wang et al.*, 2002] and the onset of Indochina extrusion by ~35 Ma [*Leloup et al.*, 2007; *Leloup et al.*, 1995; *Tapponnier et al.*, 1990]. In contrast, a continent-continent collision soon after ~60 Ma as proposed by the conventional models requires extreme shortening of Lhasa, an extremely large Greater India and a 20 Myr time lag to account for these major events recorded in the regional geology.

Acknowledgements

Numerical models were run on the CiTerra cluster at Caltech and the Australian National Computational Infrastructure (NCI). CitcomS was obtained from the Computational Infrastructure for Geodynamics (www.geodynamics.org). All figures were created using GPlates (www.gplates.org) and Generic Mapping Tools (GMT, gmt.soest.hawaii.edu). This project was supported by Statoil and ARC grants FL0992245 and DP0987713, the National Science Foundation under EAR-0810303, and by the Gordon and Betty Moore Foundation (through the Caltech Tectonics Observatory). We are thankful for the constructive suggestions of two anonymous reviewers and the Editors that considerably improved the original manuscript.

Figure Captions

Figure 1. Regional geology related to the India-Eurasia collision, showing Tethyan suture zones, magmatic episodes and major faults [*McDermid et al.*, 2002; *Styron et al.*, 2010].

Figure 2. India-Eurasia convergence rates derived at 1 Myr intervals from the motion of a present-day reference point (30°N, 80°E) using alternative rotation models that were standardised to the time scale of *Cande and Kent* [1995]. The initial drop in convergence rates varies from ~58 Ma in the *Lee and Lawver* (1995) model, to ~58 and ~48 Ma in the model of *Molnar and Stock* (2009), while the model of *Müller et al.* (2008) suggests initial convergence rate drop at ~55 Ma. Thus the interpretation of collision timing purely from convergence rates is largely model-dependent, with a 10 Myr range of initial collision timing just from four rotation models.

Figure 3. Timing of contact implied by different rotation models with the conventional pre-collision geometries of Greater India [*Lee and Lawver*, 1995] and Andean-style Eurasian margin. A number of rotation models were implemented for India, standardised to a common time scale [*Cande and Kent*, 1995] and with a fixed Eurasia. A number of other subduction zone paleo-locations are plotted for comparison, highlighting that the choice of pre-collision margins has a more significant effect on collision timing than the choice of rotation models alone. The choice of Eurasian margin geometries result in ~15 Myr timing difference of the initial contact between Greater India and Eurasia whereas the different rotation models can only account for ~5 Myr difference in interpreting initial collision based on an Andean-style convergence history for the NeoTethys. The collision between Greater India and Lhasa (green) occurs at ~55 Ma in the *Lee and Lawver* (1995) model. We chose to largely follow the subduction zone location as proposed by *Replumaz et al.* (2004) for pre-collision times in the conventional Andean-style margin, with the

Lee and Lawver (1995) extent of Greater India resulting in continental contact at ~58 Ma. Light grey shading represents extent of Eurasian continental crust in our model.

Figure 4. Pre-breakup Gondwana fit (fixed Australia) at 140 Ma with present-day *Sandwell and Smith* (1997) 1-min gravity anomaly grid. The conventional model (*Lee and Lawver* [1995]) proposes a large hypothetical extent of Greater India [black line]. The alternative model invokes a smaller Greater India [orange line] limited in extent by the Gondwana pre-breakup fit and the Wallaby Zenith Fracture Zone (WZFZ) [white line]. India rotated counter-clockwise away from Australia, followed by a northward advance that is highlighted by the Indian Ocean fracture zone bends.

Figure 5. End-member kinematic models, conventional model [left] and alternative model [right], with plate velocities, block outlines, plate boundaries and seafloor age-grids. The conventional model implies northward dipping Andean-style subduction along southern Eurasia to consume the Paleo-, Meso- and Neo- Tethys. The alternative model invokes back-arc spreading from 150 to 120 Ma in the central MesoTethys. Argoland (West Burma Block) accretes to Eurasia by 80 Ma in both scenarios. Greater India collides with Eurasia by 55 Ma in the conventional model to terminate NeoTethyan subduction. The NeoTethyan island arc is accreted onto a smaller Greater India by ~58 Ma in the alternative model, after which the associated back-arc is subducted along an Andean-style margin until continental collision between Indian and Eurasia by ~40 Ma.

Figure 6. Effect of absolute reference frames on past locations of subduction in the Tethys and northwest Pacific. Present-day coastlines are plotted only for reference. Latitudinal position of Tethyan subduction varies by up to 10° latitude across different absolute reference frame at ~200 Ma. From 150 Ma, moving hotspot and true polar wander-corrected reference frame

(MHS/TPW) is similar to the fixed hotspot reference (FHS), with the subduction reference frame (VMSR) differing largely in longitudinal position. [Orthographic projection, centred: 0°N, 90°E]

Figure 7. Plate reconstructions with age-coded mantle seismic tomography (MIT-P and GRAND-S), applying an average slab sinking rate of 3 and 1.2 cm/yr in the upper and lower mantle respectively, as an independent constraint on the southward extent of the NeoTethyan back-arc basin at pre-collision times. Location of northward-dipping subduction along continental Eurasia in the conventional scenario (left column) does not account for the large positive seismic velocity anomaly at pre-collision times, while a subduction zone offset further south in the central Meso- and Neo- Tethys in the alternative scenario (right column) better describes the P- and S- wave tomographic observations, assuming near-vertical sinking slabs. Reconstructed Coastlines/Block outlines – grey, GI – Greater India, MT – MesoTethys, NT - NeoTethys. [Orthographic projection, centred: 0°N, 90°E]

Figure 8. Model horizontal average non-dimensional temperature (left) and viscosity (right) with depth for the initial condition (red) and present-day (black).

Figure 9. Time-dependent horizontal slices (328 km) of predicted temperature field with plate boundary configurations and the location of vertical slices (orange – static great circle segment between 10°S, 55°E and 45°N, 90°E) documenting mantle evolution resulting from Tethyan plate motions. a) Initial condition between 200 and 150 Ma depicting the accretion of Cimmerian terranes of Iran, Afghanistan, South Tibet (Lhasa) and Sibumasu onto the Eurasian margin in the late Jurassic with Andean-style subduction at ~30°N. b) Conventional models of Meso- and Neo-Tethyan evolution have continuous Andean-style subduction, with collision between India and Eurasia at ~55 Ma where subduction of oceanic lithosphere ceases and a single slab descends towards the CMB at ~25°N. c) Equivalent vertical slice through the alternative scenario highlights

the different location of subduction in the Meso- and Neo- Tethys during the opening of the back-arc between 150 and 120 Ma, shifting subduction south to ~10°N between 120 and 60 Ma. Slab penetration is slowed at the upper/lower mantle transition zone, with a mantle avalanche occurring after 90 Ma. A smaller Greater India collides with the island arc to consume the back-arc basin along continental Eurasia (southern Lhasa) between ~55 and 40 Ma, resulting in two discrete slab volumes at ~10°N and ~25°N at mid-mantle depths by 30 Ma. PaleoTethyan material subducted originally at ~30°N in both scenarios migrates gradually southward due to the return flow at mid- and lower-mantle depths.

Figure 10. a) Present-day temperature field predicted by numerical models along a vertical profile (magenta line - location of vertical, great circle segment between 10°S, 55°E and 45°N, 90°E), with slabs defined as thermal anomalies colder than 10% of the ambient mantle temperature. b) Present-day mantle structure from a range of P- and S-wave mantle tomographic models along equivalent vertical slices, with slab contours from numerical models of the conventional (red) and alternative (green) models of India-Eurasia collision. The conventional model predictions do not account for the large latitudinal range of seismic velocity anomalies at mid-mantle depths. Tomographic models suggest the existence of a slab at ~1000 km depth at near-equatorial latitudes, and a larger mid-mantle slab ranging from 5 to 35°N. The conventional scenario only reproduces the larger slab, and does not account for the large latitudinal range of seismic velocity anomalies that are better reproduced by the alternative scenario invoking intra-oceanic subduction in the Meso- and Neo-Tethys.

Figure 11. Comparison of depth slices from P- and S- wave models with slab contours at similar depths from conventional (red) and alternative (green) subduction model outputs. Present-day coastlines are plotted for reference (dark grey). Positive seismic velocity anomalies better correlate with the alternative scenario slab contours to reproduce the discrete slab volumes and the large latitudinal range. At depths of ~1200 and ~1300 km, the discrete slab volume predicted by the

alternative scenario is also observable in tomography, with a systematic ~10° longitudinal offset in some tomographic models. A depth slice at ~1300 km was not available for the GRAND-S model, and so the closest slice of 1445 km was included. [Mercator projection]

Figure 12. Time-dependent mantle flow predicted by the conventional (left) and alternative (right) scenarios of India-Eurasia convergence at 30 Myr increments between 90 and 0 Ma at a depth of 1012 km. Predicted lateral flow is denoted by grey arrows, and the north-south component is highlighted by larger red arrows. A strong southward component in the return flow at this depth is predicted at 90 and 0 Ma. [Albers projection, centre: 25°N, 80°E, standard parallels: 10 and 40°N]

Tables

Table 1. Collision timing between India and an Andean-style margin of Eurasia as inferred from the contact of maximum extent Greater India (*Lee and Lawver*, 1995) and a range of southern Eurasian margins using different rotation models that were standardised to the time scale of *Cande and Kent* (1995). Timing offset is a maximum of 4 Myr for each proposed margin, but 15 Myr when comparing all margins – showing that the pre-collision margin choice has the biggest impact on the interpretation of collision timing rather than the choice of motion models of India relative to Eurasia.

		South Eurasian Andean-style margin			
		Tapponnier et al. (1986)	*Lee and Lawver* (1995)	*Norton* (1999)	*Replumaz et al*. (2004)
Rotation Model	*Müller et al*. (2008) – this study	61 Ma	53 Ma	53 Ma	55 Ma
	van Hinsbergen et al. (2011)	61 Ma	53 Ma	53 Ma	55 Ma
	Molnar and Stock (2009)	60 Ma	49 Ma	50 Ma	53 Ma
	Lee and Lawver (1995)	64 Ma	54 Ma	53 Ma	57 Ma

Table 2. Vertical and lateral mesh resolution in *CitcomS* models

		Average Resolution
Vertical	Upper mantle	26 km
	Lower mantle	56 km
Lateral	Surface	50 km
	Core-mantle boundary	23 km

Table 3. Numerical model parameters

Constant variables	
Reference density, ρ_0	4000 kg/m^3
Reference viscosity, η_0	1×10^{21} Pa s
Activation energy (upper mantle), E_η	100 kJ/mol
Activation energy (lower mantle), E_η	33 kJ/mol
Activation temperature, T_η	225 K
Thermal diffusivity, κ	1×10^{-6} m^2/s
Coefficient of thermal expansion, α	3×10^{-5} K^{-1}
Earth radius, R	6371 km
Gravitational acceleration, g	9.81 m/s^2
Temperature contrast, ΔT	1400 K

References

Acharyya, S. (1998), Break-up of the greater Indo-Australian continent and accretion of blocks framing south and east Asia, *Journal of Geodynamics*, *26*(1), 149-170.

Aitchison, J., J. Ali, and A. Davis (2007), When and where did India and Asia collide?, *Journal of Geophysical Research*, *112*, 1-19.

Aitchison, J., X. Xia, A. Baxter, and J. Ali (2011), Detrital zircon U-Pb ages along the Yarlung-Tsangpo suture zone, Tibet: Implications for oblique convergence and collision between India and Asia, *Gondwana Research*, *20*(4), 691-709.

Aitchison, J., A. Davis, J. Liu, H. Luo, J. Malpas, I. McDermid, H. Wu, S. Ziabrev, and M. Zhou (2000), Remnants of a Cretaceous intra-oceanic subduction system within the Yarlung-Zangbo suture (southern Tibet), *Earth and Planetary Science Letters*, *183*(1-2), 231-244.

Aitchison, J. C., X. Xia, A. T. Baxter, and J. R. Ali (2011), Detrital zircon U-Pb ages along the Yarlung-Tsangpo suture zone, Tibet: Implications for oblique convergence and collision between India and Asia, *Gondwana Research*, *20*(4), 691-709.

Ali, J., and J. Aitchison (2005), Greater India, *Earth-Science Reviews*, *72*(3-4), 169-188.

Ali, J., and J. Aitchison (2008), Gondwana to Asia: Plate tectonics, paleogeography and the biological connectivity of the Indian sub-continent from the Middle Jurassic through latest Eocene (166-35 Ma), *Earth-Science Reviews*, *88*(3-4), 145-166.

Allegre, C., V. Courtillot, P. Tapponnier, A. Hirn, M. Mattauer, C. Coulon, J. Jaeger, J. Achache, U. Scharer, and J. Marcoux (1984), Structure and evolution of the Himalaya-Tibet orogenic belt, *Nature*, *307*, 17-22.

Alpert, L., T. Becker, and I. Bailey (2010), Global slab deformation and centroid moment tensor constraints on viscosity, *Geochemistry, Geophysics, Geosystems*, *11*(12), 1-22.

Artemieva, I. M. (2006), Global 1° X 1° thermal model TC1 for the continental lithosphere: Implications for lithosphere secular evolution, *Tectonophysics*, *416*(1-4), 245-277.

Artemieva, I. M. (2009), The continental lithosphere: reconciling thermal, seismic, and petrologic data, *Lithos*, *109*(1-2), 23-46.

Becker, T., and L. Boschi (2002), A comparison of tomographic and geodynamic mantle models, *Geochemistry, Geophysics, Geosystems*, *3*(1), 1003.

Bercovici, D., Y. Ricard, and M. Richards (2000), The relation between mantle dynamics and plate tectonics: A primer, *Geophysical Monograph*, *121*, 5-46.

Bijwaard, H., W. Spakman, and E. Engdahl (1998), Closing the gap between regional and global travel time tomography, *Journal of Geophysical Research*, *103*(B12), 30055.

Cande, S. C., and D. V. Kent (1995), Revised calibration of the geomagnetic polarity timescale for the Late Cretaceous and Cenozoic, *Journal of Geophysical Research*, *100*(B4), 3.

Cande, S. C., and D. R. Stegman (2011), Indian and African plate motions driven by the push force of the Reunion plume head, *Nature*, *475*(7354), 47-52.

Cande, S. C., P. Patriat, and J. Dyment (2010), Motion between the Indian, Antarctic and African plates in the early Cenozoic, *Geophysical Journal International*(183), 127-149.

Chung, S., M. Chu, Y. Zhang, Y. Xie, C. Lo, T. Lee, C. Lan, X. Li, Q. Zhang, and Y. Wang (2005), Tibetan tectonic evolution inferred from spatial and temporal variations in post-collisional magmatism, *Earth-Science Reviews*, *68*(3-4), 173-196.

Clark, S. R., D. Stegman, and R. Müller (2008), Episodicity in back-arc tectonic regimes, *Physics of The Earth and Planetary Interiors*, *171*(1-4), 265-279.

Clift, P., A. Carter, M. Krol, and E. Kirby (2002), Constraints on India-Eurasia collision in the Arabian sea region taken from the Indus Group, Ladakh Himalaya, India, *Geological Society, London, Special Publications*, *195*(1), 97.

Cottle, J., M. Searle, M. Horstwood, and D. Waters (2009), Timing of midcrustal metamorphism, melting, and deformation in the Mount Everest Region of southern Tibet revealed by U (-Th)-Pb geochronology, *The Journal of geology*, *117*(6), 643-664.

Davis, A., J. Aitchison, H. Luo, and S. Zyabrev (2002), Paleogene island arc collision-related conglomerates, Yarlung-Tsangpo suture zone, Tibet, *Sedimentary Geology*, *150*(3-4), 247-273.

Debon, F., P. Le Fort, S. Sheppard, and J. Sonet (1986), The four plutonic belts of the trans-Himalaya: A chemical, mineralogical, isotopic and chronological synthesis along a Tibet-Nepal section, *Journal of Petrology*, *27*, 219-250.

Dewey, J., R. Shackleton, C. Chengfa, and S. Yiyin (1988), The tectonic evolution of the Tibetan Plateau, *Philosophical Transactions of the Royal Society of London. Series A, Mathematical and Physical Sciences*, *327*(1594), 379-413.

Dumitru, T., D. Zhou, E. Chang, S. Graham, M. Hendrix, E. Sobel, and A. Carroll (2001), Uplift, exhumation, and deformation in the Chinese Tian Shan, in *Paleozoic and Mesozoic tectonic evolution of central Asia: from continental assembly to intracontinental deformation*, edited, pp. 71-99, Geological Society of America.

Dupont-Nivet, G., P. C. Lippert, D. Van Hinsbergen, M. J. M. Meijers, and P. Kapp (2010), Palaeolatitude and age of the Indo-Asia collision: palaeomagnetic constraints, *Geophys. J. Int*, *182*, 1189-1198.

Gaetani, M., and E. Garzanti (1991), Multicyclic history of the northern India continental margin (northwestern Himalaya), *AAPG Bull*, *75*(9), 1427-1446.

Garzanti, E. (2008), Comment on" When and where did India and Asia collide?" by Jonathan C. Aitchison, Jason R. Ali, and Aileen M. Davis *Journal of Geophysical Research - Solid Earth*, *113*, 4.

Golonka, J. (2004), Plate tectonic evolution of the southern margin of Eurasia in the Mesozoic and Cenozoic, *Tectonophysics*, *381*(1-4), 235-273.

Grand, S. (2002), Mantle shear-wave tomography and the fate of subducted slabs, *Philosophical Transactions of the Royal Society of London. Series A: Mathematical, Physical and Engineering Sciences*, *360*(1800), 2475.

Gurnis, M., M. Turner, S. Zahirovic, L. DiCaprio, S. Spasojevic, R. Müller, J. Boyden, M. Seton, V. Manea, and D. Bower (2012), Plate Tectonic Reconstructions with Continuously Closing Plates, *Computers & Geosciences*, *38*(1), 35-42.

Hafkenscheid, E., M. Wortel, and W. Spakman (2006), Subduction history of the Tethyan region derived from seismic tomography and tectonic reconstructions, *Journal of Geophysical Research-Solid Earth*, *111*(B8), B08401.

Hager, B. H. (1984), Subducted slabs and the geoid: constraints on mantle rheology and flow, *Journal of Geophysical Research*, *89*(B7), 6003-6015.

Heine, C., and R. Müller (2005), Late Jurassic rifting along the Australian North West Shelf: margin geometry and spreading ridge configuration, *Australian Journal of Earth Sciences*, *52*(1), 27-39.

Henderson, A., Y. Najman, R. Parrish, D. Mark, and G. Foster (2011), Constraints to the timing of India-Eurasia collision; a re-evaluation of evidence from the Indus Basin sedimentary rocks of the Indus-Tsangpo Suture Zone, Ladakh, India, *Earth-Science Reviews*, *106*(3-4), 265-292.

Jarvis, G., and J. Lowman (2005), Sinking slabs below fossil subduction zones, *Physics of The Earth and Planetary Interiors*, *152*(1-2), 103-115.

Jarvis, G., and J. Lowman (2007), Survival times of subducted slab remnants in numerical models of mantle flow, *Earth and Planetary Science Letters*, *260*(1-2), 23-36.

Khan, S., D. Walker, S. Hall, K. Burke, M. Shah, and L. Stockli (2009), Did the Kohistan-Ladakh island arc collide first with India?, *Geological Society of America Bulletin*, *121*(3-4), 366.

Khan, T., M. Murata, T. Karim, M. Zafar, and H. Ozawa (2007), A Cretaceous dike swarm provides evidence of a spreading axis in the back-arc basin of the Kohistan paleo-island arc, northwestern Himalaya, Pakistan, *Journal of Asian Earth Sciences*, *29*(2-3), 350-360.

Klootwijk, C., and P. Conaghan (1979), The extent of Greater India, I. Preliminary palaeomagnetic data from the Upper Devonian of the eastern Hindukush, Chitral (Pakistan), *Earth and Planetary Science Letters*, *42*(2), 167-182.

Klootwijk, C., P. Conaghan, and C. Powell (1985), The Himalayan Arc: large-scale continental subduction, oroclinal bending and back-arc spreading, *Earth and Planetary Science Letters*, *75*(2-3), 167-183.

Lee, T.-Y., and L. A. Lawver (1995), Cenozoic plate reconstruction of Southeast Asia, *Tectonophysics*, *251*(1-4), 85-138.

Leloup, P., P. Tapponnier, and R. Lacassin (2007), Discussion on the role of the Red River shear zone, Yunnan and Vietnam, in the continental extrusion of SE Asia, *Journal of the Geological Society*, *164*, 1253-1260.

Leloup, P., R. Lacassin, P. Tapponnier, and U. Schärer (1995), The Ailao Shan-Red River shear zone (Yunnan, China), Tertiary transform boundary of Indochina, *Tectonophysics*, *251*(1-4), 3-10.

Leloup, P., N. Arnaud, R. Lacassin, J. Kienast, T. Harrison, T. T. P. Trong, A. Replumaz, and P. Tapponnier (2001), New constraints on the structure, thermochronology, and timing of the Ailao Shan-Red River shear zone, SE Asia, *Journal of Geophysical Research*, *106*(B4), 6683-6732.

Li, C., R. van der Hilst, E. Engdahl, and S. Burdick (2008), A new global model for P wave speed variations in Earth's mantle, *Geochemistry, Geophysics, Geosystems*, *9*(Q05018), 21.

Lippert, P. C., X. Zhao, R. S. Coe, and C. H. Lo (2011), Palaeomagnetism and 40Ar/39Ar geochronology of upper Palaeogene volcanic rocks from Central Tibet: implications for the Central Asia inclination anomaly, the palaeolatitude of Tibet and post 50 Ma shortening within Asia, *Geophysical Journal International*, *184*(2), 131-161.

Liu, L., and M. Gurnis (2008), Simultaneous inversion of mantle properties and initial conditions using an adjoint of mantle convection, *Journal of Geophysical Research B*, *113*(B08405), 17.

Liu, Y. J., F. Neubauer, J. Genser, X. H. Ge, A. Takasu, S. H. Yuan, L. H. Chang, and W. M. Li (2007), Geochronology of the initiation and displacement of the Altyn Strike-Slip Fault, western China, *Journal of Asian Earth Sciences*, *29*(2-3), 243-252.

Masters, G., G. Laske, H. Bolton, and A. Dziewonski (2000), The relative behavior of shear velocity, bulk sound speed, and compressional velocity in the mantle: implications for chemical and thermal structure, *Geophysical Monograph*, *117*, 63-88.

Matthews, K. J., A. J. Hale, M. Gurnis, R. Müller, and L. DiCaprio (2011), Dynamic subsidence of Eastern Australia during the Cretaceous, *Gondwana Research*, *19*(2), 373-383.

McDermid, I., J. Aitchison, A. Davis, T. Harrison, and M. Grove (2002), The Zedong terrane: a Late Jurassic intra-oceanic magmatic arc within the Yarlung-Tsangpo suture zone, southeastern Tibet, *Chemical Geology*, *187*(3-4), 267-277.

Miller, C., R. Schuster, U. Klotzli, W. Frank, and F. Purtscheller (1999), Post-collisional potassic and ultrapotassic magmatism in SW Tibet: Geochemical and Sr-Nd-Pb-O isotopic constraints for mantle source characteristics and petrogenesis, *Journal of Petrology*, *40*(9), 1399.

Molnar, P., and J. Stock (2009), Slowing of India's convergence with Eurasia since 20 Ma and its implications for Tibetan mantle dynamics, *Tectonics*, *28*(3).

Müller, R., J. Royer, and L. Lawver (1993), Revised plate motions relative to the hotspots from combined Atlantic and Indian Ocean hotspot tracks, *Geology*, *21*(3), 275.

Müller, R., C. Gaina, W. Roest, and D. Hansen (2001), A recipe for microcontinent formation, *Geology*, *29*(3), 203.

Müller, R., M. Sdrolias, C. Gaina, and W. Roest (2008), Age, spreading rates, and spreading asymmetry of the world's ocean crust, *Geochemistry, Geophysics, Geosystems*, *9*(Q04006), 19.

Najman, Y., and E. Garzanti (2000), Reconstructing early Himalayan tectonic evolution and paleogeography from Tertiary foreland basin sedimentary rocks, northern India, *Geological Society of America Bulletin*, *112*(3), 435-449.

O'Neill, C., R. Müller, and B. Steinberger (2005), On the uncertainties in hot spot reconstructions and the significance of moving hot spot reference frames, *Geochemistry, Geophysics, Geosystems*, *6*(4).

Patriat, P., and J. Achache (1984), India-Eurasia collision chronology has implications for crustal shortening and driving mechanism of plates, *Nature*, *311*, 615-621.

Pearce, J., T. Alabaster, A. Shelton, and M. Searle (1981), The Oman ophiolite as a Cretaceous arc-basin complex: evidence and implications, *Philosophical Transactions of the Royal Society of London. Series A, Mathematical and Physical Sciences*, *300*(1454), 299-317.

Pudsey, C. J. (1986), The Northern Suture, Pakistan: margin of a Cretaceous island arc, *Geological Magazine*, *123*(4), 405-423.

Raymo, M., and W. Ruddiman (1992), Tectonic forcing of late Cenozoic climate, *Nature*, *359*(6391), 117-122.

Replumaz, A., and P. Tapponnier (2003), Reconstruction of the deformed collision zone Between India and Asia by backward motion of lithospheric blocks, *Journal of Geophysical Research*, *108*(B6), 2285.

Replumaz, A., A. Negredo, S. Guillot, and A. Villasenor (2010), Multiple episodes of continental subduction during India/Asia convergence: Insight from seismic tomography and tectonic reconstruction, *Tectonophysics*, *483*(1-2), 125-134.

Replumaz, A., H. Karason, R. van der Hilst, J. Besse, and P. Tapponnier (2004), 4-D evolution of SE Asia's mantle from geological reconstructions and seismic tomography, *Earth and Planetary Science Letters*, *221*(1-4), 103-115.

Ricard, Y., M. Richards, C. Lithgow-Bertelloni, and Y. Le Stunff (1993), A geodynamic model of mantle density heterogeneity, *Journal of Geophysical Research*, *98*(B12), 21895-21821,21909.

Robb, M. S., B. Taylor, and A. M. Goodliffe (2005), Re examination of the magnetic lineations of the Gascoyne and Cuvier Abyssal Plains, off NW Australia, *Geophysical Journal International*, *163*(1), 42-55.

Romanowicz, B. (2008), Using seismic waves to image Earth's internal structure, *Nature*, *451*(7176), 266-268.

Rowley, D. (1996), Age of initiation of collision between India and Asia: A review of stratigraphic data, *Earth and Planetary Science Letters*, *145*(1-4), 1-13.

Roy, S. S. (1976), A possible Himalayan microcontinent, *Nature*, *263*.

Searle, M., et al. (1987), The closing of the Tethys and the tectonics of the Himalaya, *Geological Society of America Bulletin*, *98*.

Seton, M., M. R.D., S. Zahirovic, C. Gaina, T. Torsvik, S. G., A. Talsma, M. Gurnis, and M. Turner (submitted), Global continental and ocean basin reconstructions.

Shervais, J. (2001), Birth, death, and resurrection: The life cycle of suprasubduction zone ophiolites, *Geochemistry, Geophysics, Geosystems*, *2*(1), 45.

Simmons, N., A. Forte, and S. Grand (2009), Joint seismic, geodynamic and mineral physical constraints on three-dimensional mantle heterogeneity: Implications for the relative importance of thermal versus compositional heterogeneity, *Geophysical Journal International*, *177*(3), 1284-1304.

Stampfli, G. M., and G. D. Borel (2002), A plate tectonic model for the Paleozoic and Mesozoic constrained by dynamic plate boundaries and restored synthetic oceanic isochrons, *Earth and Planetary Science Letters*, *196*(1-2), 17-33.

Steinberger, B., and T. Torsvik (2008), Absolute plate motions and true polar wander in the absence of hotspot tracks, *Nature*, *452*(7187), 620-623.

Sun, Z., W. Jiang, H. Li, J. Pei, and Z. Zhu (2010), New paleomagnetic results of Paleocene volcanic rocks from the Lhasa block: Tectonic implications for the collision of India and Asia, *Tectonophysics*, *490*(3-4), 257-266.

Sun, Z., J. Pei, H. Li, W. Xu, W. Jiang, Z. Zhu, X. Wang, and Z. Yang (2012), Palaeomagnetism of Late Cretaceous sediments from southern Tibet: Evidence for the consistent palaeolatitudes of the southern margin of Eurasia prior to the collision with India, *Gondwana Research*, *21*, 53-63.

Tan, E., E. Choi, P. Thoutireddy, M. Gurnis, and M. Aivazis (2006), GeoFramework: Coupling multiple models of mantle convection within a computational framework, *Geochemistry, Geophysics, Geosystems*, *7*(6), Q06001.

Tan, X., S. Gilder, K. P. Kodama, W. Jiang, Y. Han, H. Zhang, H. Xu, and D. Zhou (2010), New paleomagnetic results from the Lhasa block: revised estimation of latitudinal shortening across Tibet and implications for dating the India-Asia collision, *Earth and Planetary Science Letters*, *293*(3-4), 396-404.

Tapponnier, P., G. Peltzer, A. Y. Le Dain, R. Armijo, and P. Cobbold (1982), Propagating extrusion tectonics in Asia: New insights from simple experiments with plasticine, *Geology*, *10*(12), 611-616.

Tapponnier, P., R. Lacassin, P. H. Leloup, U. Scharer, Z. Dalai, W. Haiwei, L. Xiaohan, J. Shaocheng, Z. Lianshang, and Z. Jiayou (1990), The Ailao Shan/Red River metamorphic belt: Tertiary left-lateral shear between Indochina and South China, *Nature*, *343*(6257), 431-437.

Thorkelson, D. (1995), Subduction of diverging plates and principles of slab window formation, *Tectonophysics*, *255*(1-2), 47-63.

Torsvik, T. H., B. Steinberger, M. Gurnis, and C. Gaina (2010), Plate tectonics and net lithosphere rotation over the past 150 My, *Earth and Planetary Science Letters*, *291*(1-4), 106-112.

Van Der Meer, D., W. Spakman, D. van Hinsbergen, M. Amaru, and T. Torsvik (2010), Towards absolute plate motions constrained by lower-mantle slab remnants, *Nature Geoscience*, *3*.

Van der Voo, R., W. Spakman, and H. Bijwaard (1999a), Mesozoic subducted slabs under Siberia, *Nature*, *397*(6716), 246-249.

Van der Voo, R., W. Spakman, and H. Bijwaard (1999b), Tethyan subducted slabs under India, *Earth and Planetary Science Letters*, *171*(1), 7-20.

van Hinsbergen, D., B. Steinberger, P. Doubrovine, and R. Gassmöller (2011a), Acceleration and deceleration of India-Asia convergence since the Cretaceous: roles of mantle plumes and continental collision, *Journal of Geophysical Research - Solid Earth*, *116*(B06101).

van Hinsbergen, D., P. Kapp, G. Dupont-Nivet, P. C. Lippert, P. DeCelles, and T. Torsvik (2011b), Restoration of Cenozoic deformation in Asia, and the size of Greater India, *Tectonics*, *30*(TC5003), 1-31.

Veevers, J., C. Powell, and S. Roots (1991), Review of seafloor spreading around Australia. I. Synthesis of the patterns of spreading, *Australian Journal of Earth Sciences*, *38*(4), 373-389.

Wang, C., X. Li, X. Hu, and L. Jansa (2002), Latest marine horizon north of Qomolangma (Mt Everest): implications for closure of Tethys seaway and collision tectonics, *Terra Nova*, *14*(2), 114-120.

Xia, L., X. Li, Z. Ma, X. Xu, and Z. Xia (2011), Cenozoic volcanism and tectonic evolution of the Tibetan plateau, *Gondwana Research*, *19*(4), 850-866.

Yi, Z., B. Huang, J. Chen, L. Chen, and H. Wang (2011), Paleomagnetism of early Paleogene marine sediments in southern Tibet, China: Implications to onset of the India-Asia collision and size of Greater India, *Earth and Planetary Science Letters*, *309*(1-2), 153-165.

Yin, A., and T. M. Harrison (2000), Geologic evolution of the Himalayan-Tibetan orogen, *Annual Review of Earth and Planetary Sciences*, *28*(1), 211-280.

Zhong, S., M. Zuber, L. Moresi, and M. Gurnis (2000), Role of temperature-dependent viscosity and surface plates in spherical shell models of mantle convection, *Journal of Geophysical Research*, *105*(B5), 11063.

Ziabrev, S., J. Aitchison, and A. Abrajevitch (2004), Bainang Terrane, Yarlung-Tsangpo suture, southern Tibet (Xizang, China): a record of intra-Neotethyan subduction-accretion processes preserved on the roof of the world, *Journal of the Geological Society*, *161*(3), 523.

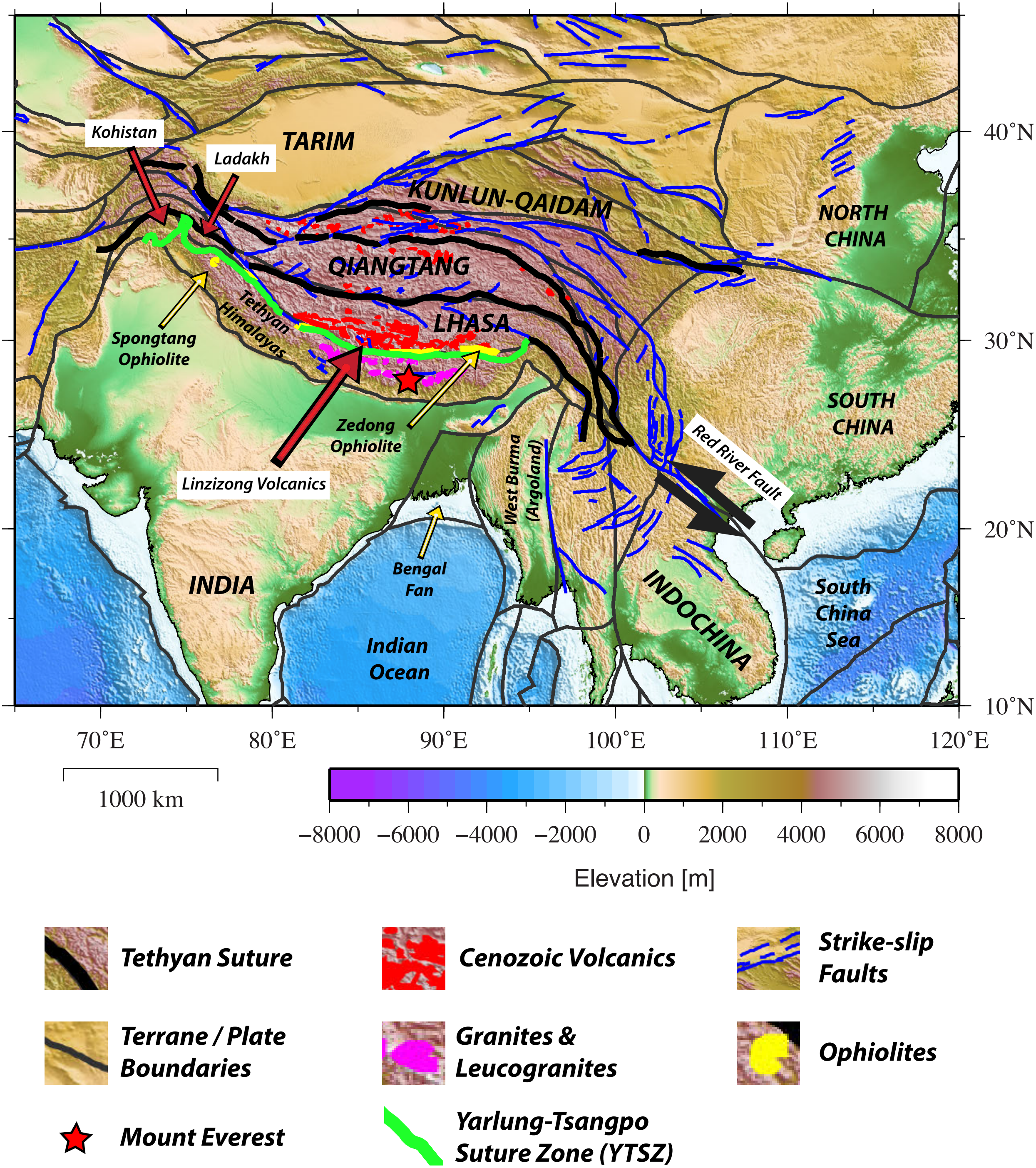

TARIM
Kohistan
Ladakh
KUNLUN-QAIDAM
NORTH CHINA
QIANGTANG
Tethyan Himalayas
LHASA
Spongtang Ophiolite
Zedong Ophiolite
Linzizong Volcanics
West Burma (Argoland)
Red River Fault
SOUTH CHINA
Bengal Fan
INDIA
INDOCHINA
South China Sea
Indian Ocean
40°N
30°N
20°N
10°N
70°E
80°E
90°E
100°E
110°E
120°E
1000 km
−8000
−6000
−4000
−2000
0
2000
4000
6000
8000
Elevation [m]
Tethyan Suture
Cenozoic Volcanics
Strike-slip Faults
Terrane / Plate Boundaries
Granites & Leucogranites
Ophiolites
Mount Everest
Yarlung-Tsangpo Suture Zone (YTSZ)

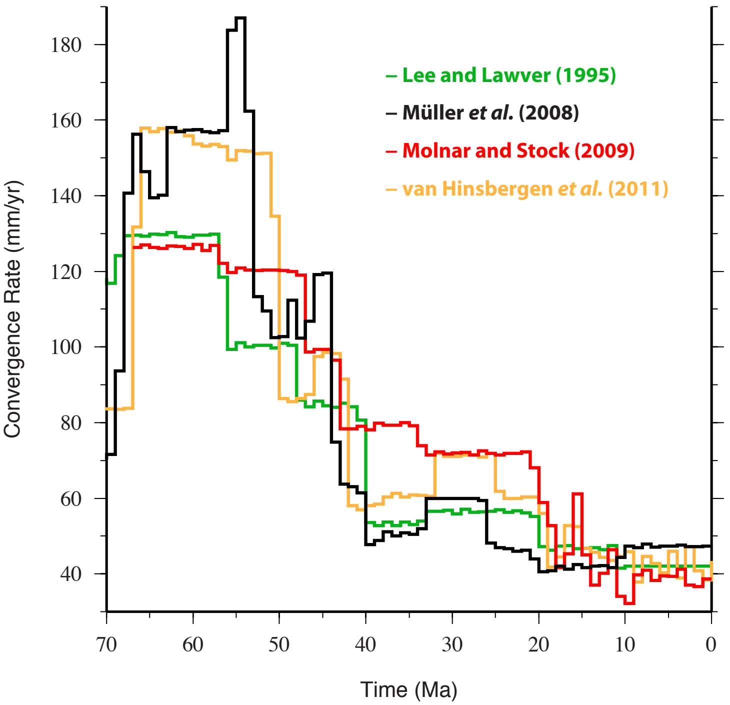
– Lee and Lawver (1995)
– Müller et al. (2008)
– Molnar and Stock (2009)
– van Hinsbergen et al. (2011)
Convergence Rate (mm/yr)
180
160
140
120
100
80
60
40
70
60
50
40
30
20
10
0
Time (Ma)

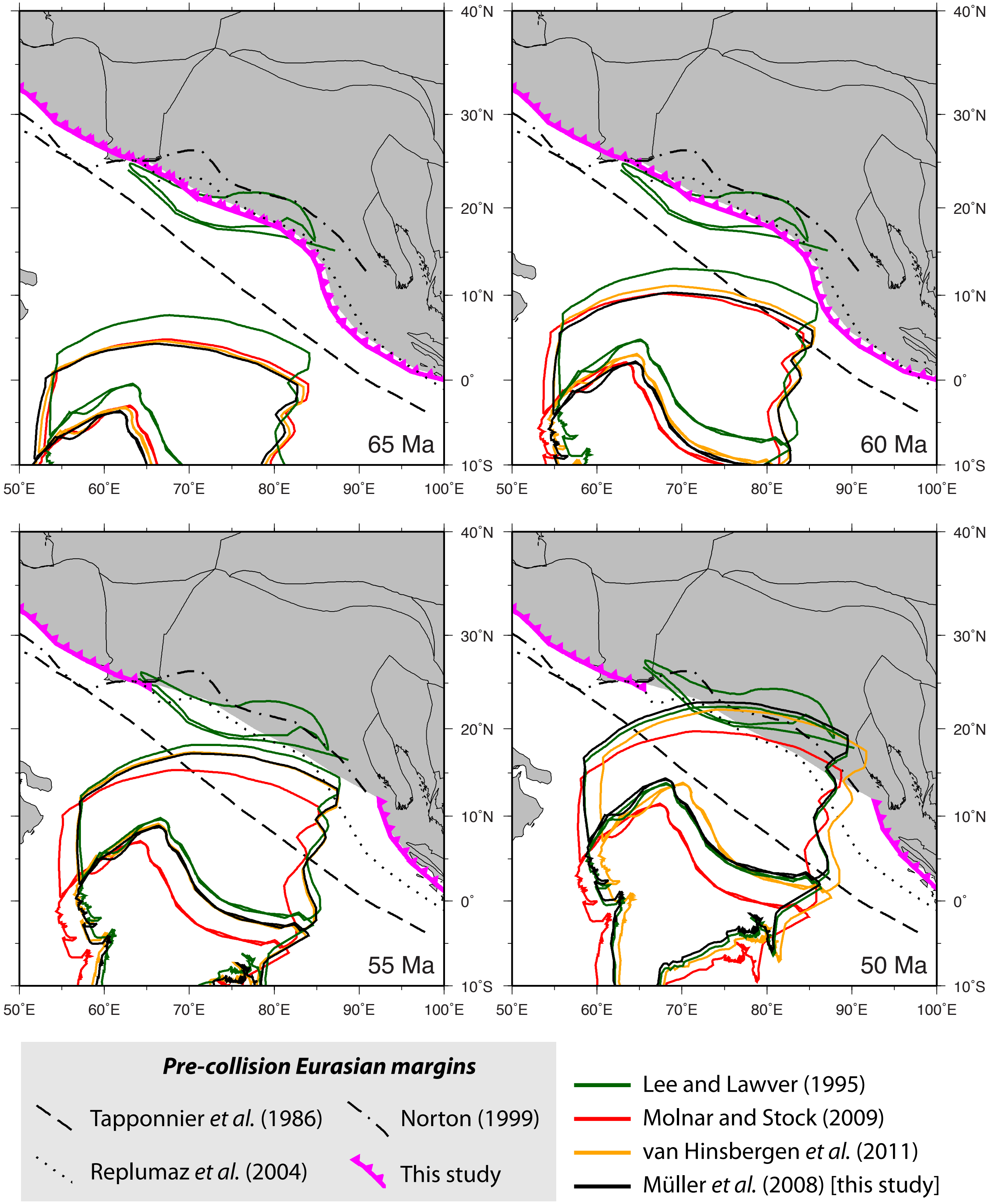
65 Ma
60 Ma
55 Ma
50 Ma
40°N
30°N
20°N
10°N
0°
10°S
50°E
60°E
70°E
80°E
90°E
100°E
Pre-collision Eurasian margins
Tapponnier et al. (1986)
Norton (1999)
Replumaz et al. (2004)
This study
Lee and Lawver (1995)
Molnar and Stock (2009)
van Hinsbergen et al. (2011)
Müller et al. (2008) [this study]

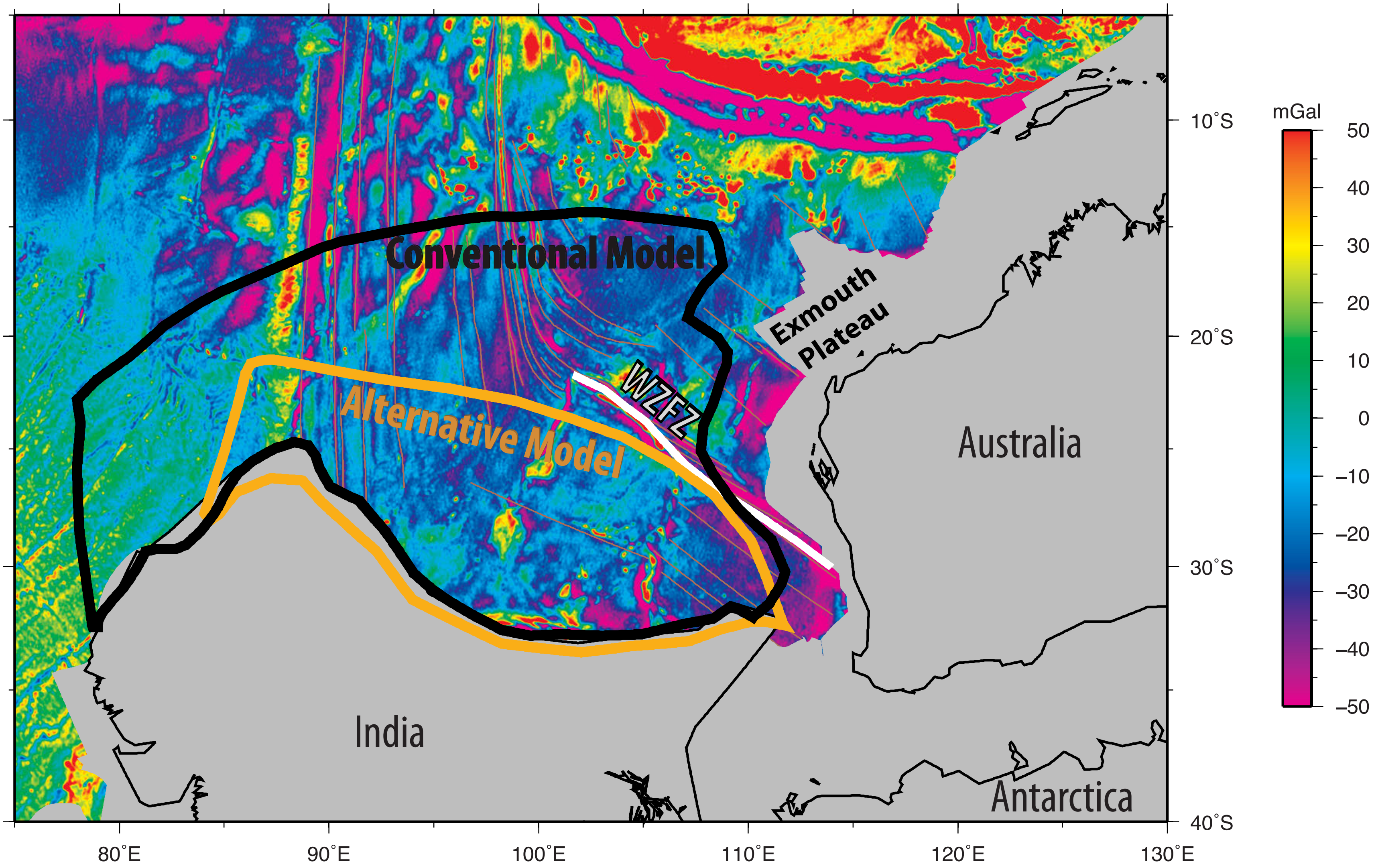
Conventional Model
Alternative Model
WZFZ
Exmouth Plateau
Australia
India
Antarctica
mGal
50
40
30
20
10
0
−10
−20
−30
−40
−50
10˚S
20˚S
30˚S
40˚S
80˚E
90˚E
100˚E
110˚E
120˚E
130˚E

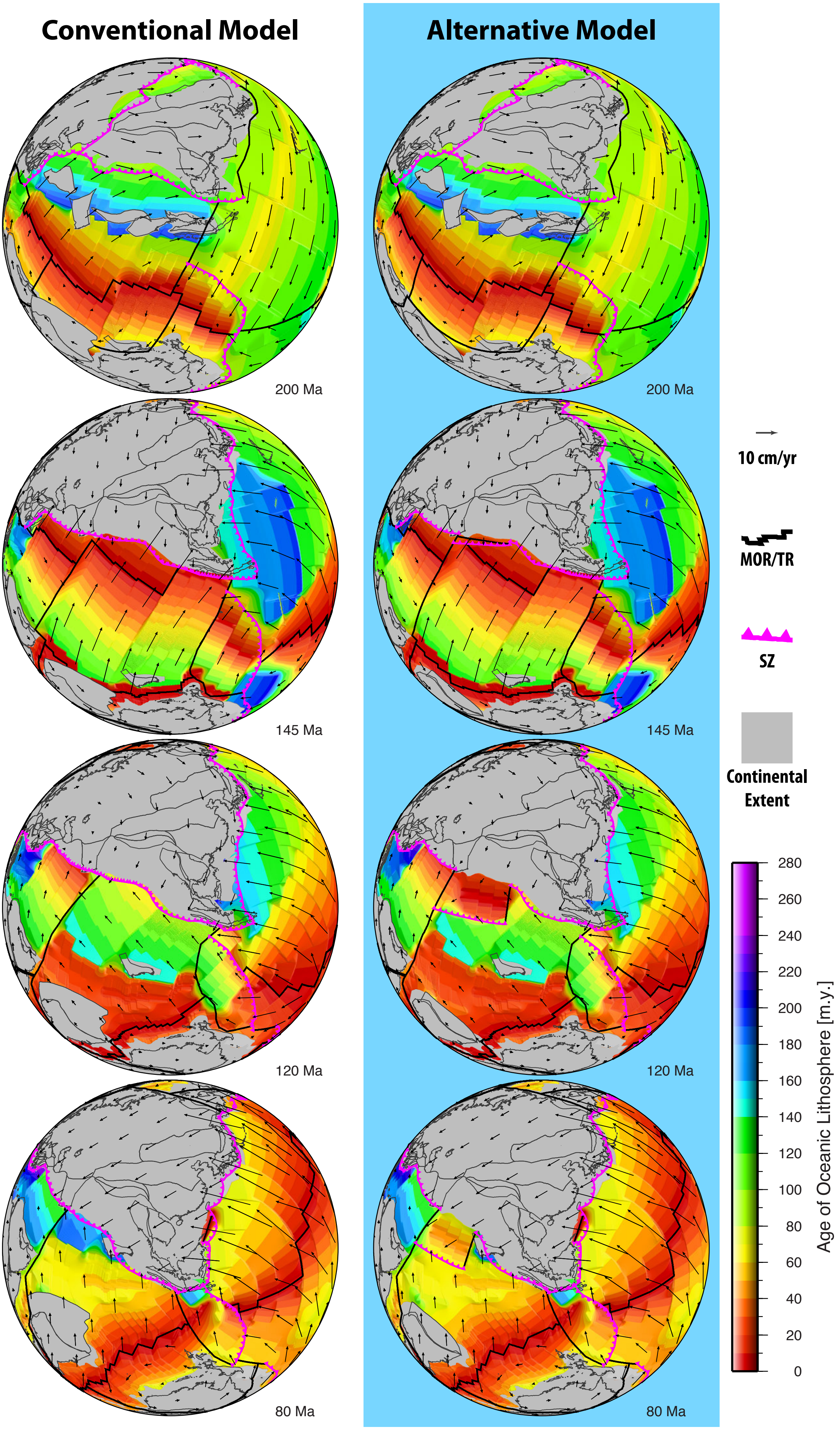

Conventional Model
Alternative Model
200 Ma
200 Ma
145 Ma
145 Ma
120 Ma
120 Ma
80 Ma
80 Ma
10 cm/yr
MOR/TR
SZ
Continental Extent
280
260
240
220
200
180
160
140
120
100
80
60
40
20
0
Age of Oceanic Lithosphere [m.y.]

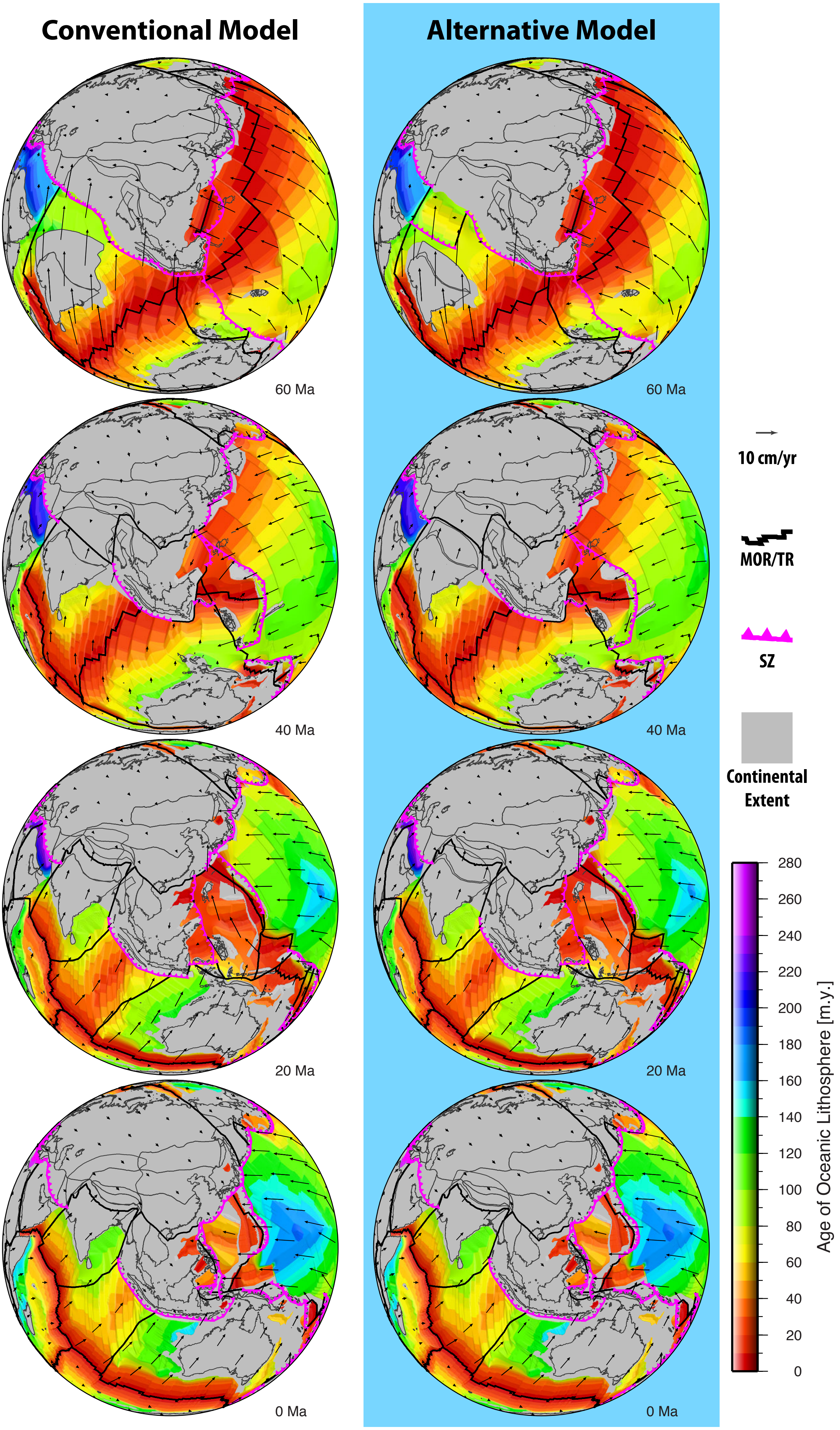

Conventional Model
Alternative Model
60 Ma
60 Ma
40 Ma
40 Ma
20 Ma
20 Ma
0 Ma
0 Ma
10 cm/yr
MOR/TR
SZ
Continental Extent
280
260
240
220
200
180
160
140
120
100
80
60
40
20
0
Age of Oceanic Lithosphere [m.y.]

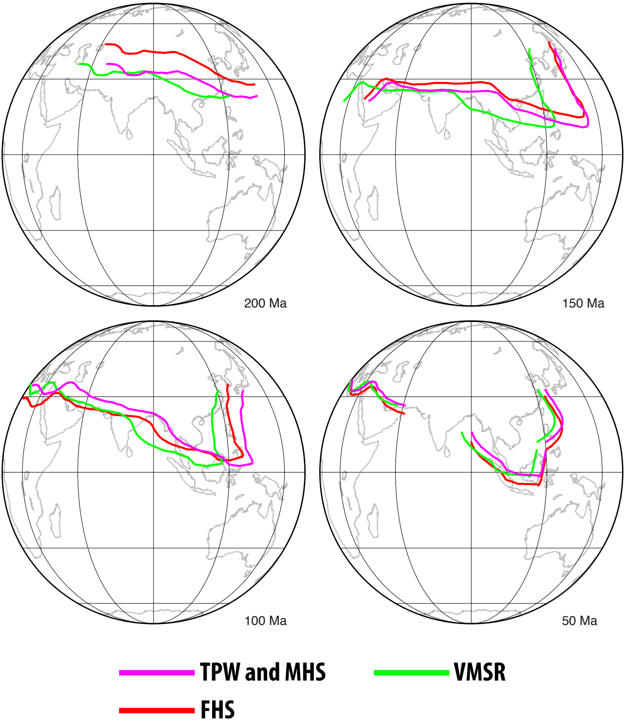
200 Ma
150 Ma
100 Ma
50 Ma
TPW and MHS
VMSR
FHS

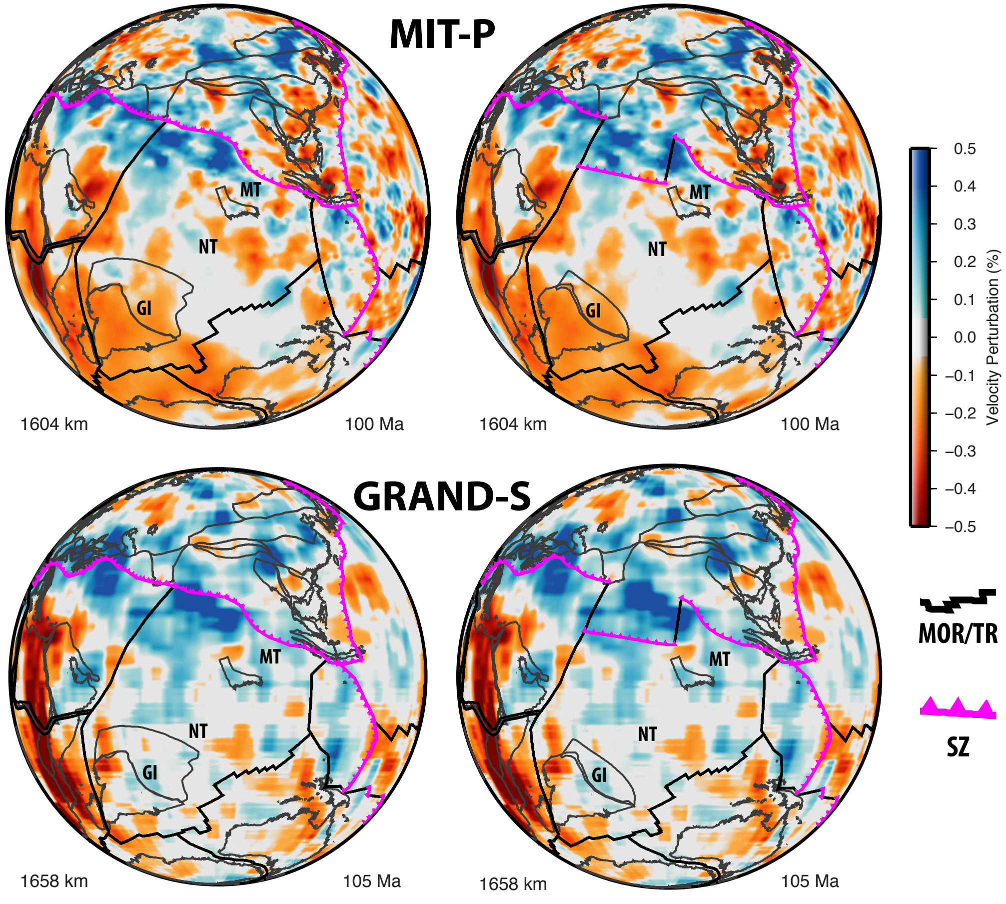

MIT-P
MT
NT
GI
1604 km
100 Ma
1604 km
100 Ma
GRAND-S
MT
NT
GI
1658 km
105 Ma
1658 km
105 Ma
0.5
0.4
0.3
0.2
0.1
0.0
−0.1
−0.2
−0.3
−0.4
−0.5
Velocity Perturbation (%)
MOR/TR
SZ

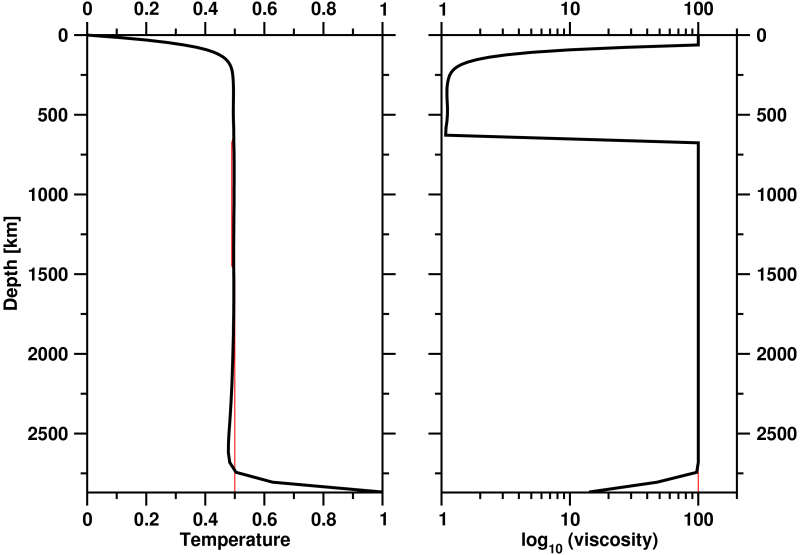

Depth [km]
Temperature
log10 (viscosity)
0
0.2
0.4
0.6
0.8
1
10
100
500
1000
1500
2000
2500

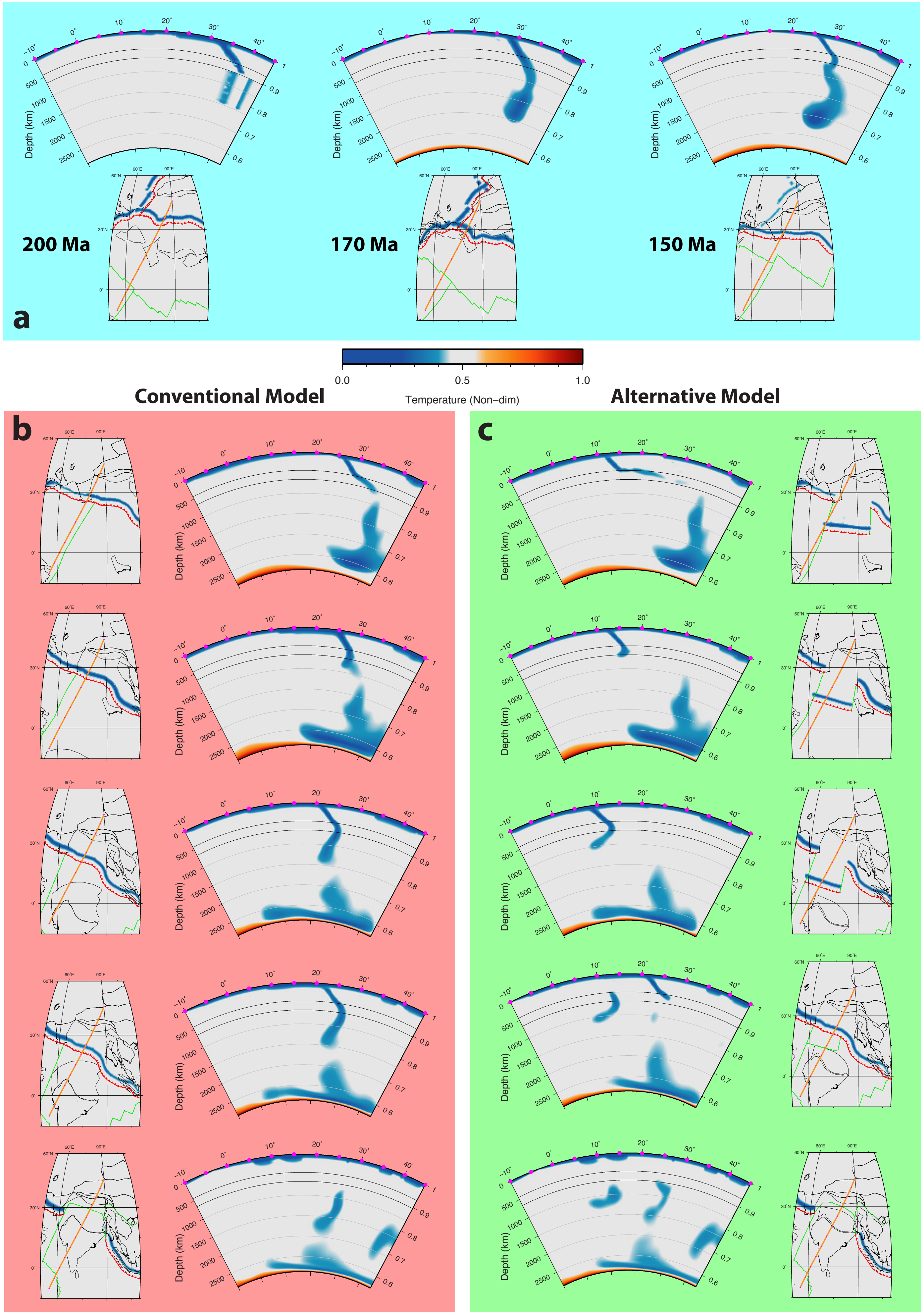

200 Ma
170 Ma
150 Ma
a
0.0
0.5
1.0
Temperature (Non–dim)
Conventional Model
Alternative Model
b
c
120 Ma
90 Ma
60 Ma
55 Ma
30 Ma
Depth (km)

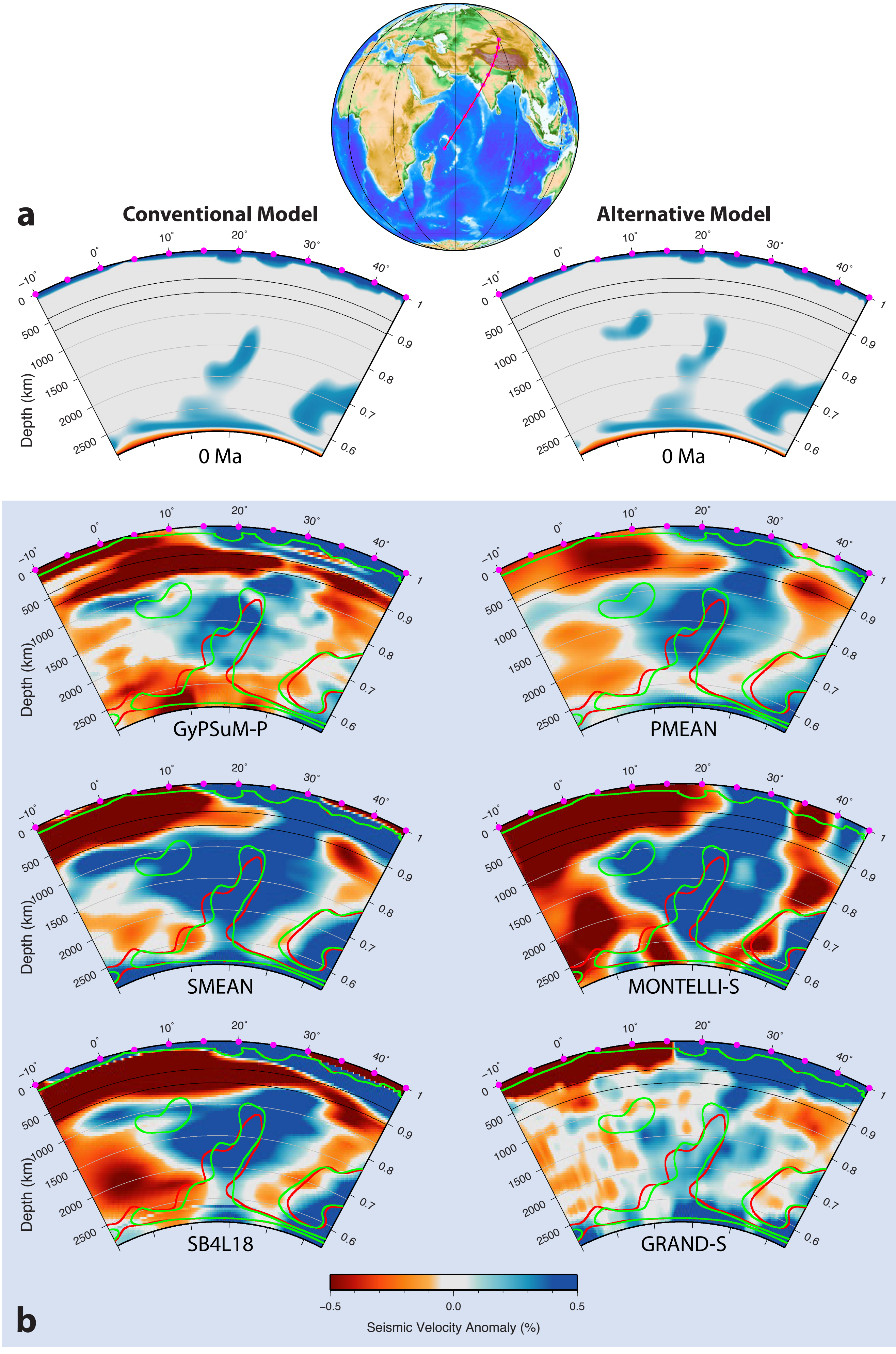
a
Conventional Model
Alternative Model
−10°
0°
10°
20°
30°
40°
0
500
1000
1500
2000
2500
Depth (km)
1
0.9
0.8
0.7
0.6
0 Ma
b
GyPSuM-P
PMEAN
SMEAN
MONTELLI-S
SB4L18
GRAND-S
−0.5
0.0
0.5
Seismic Velocity Anomaly (%)

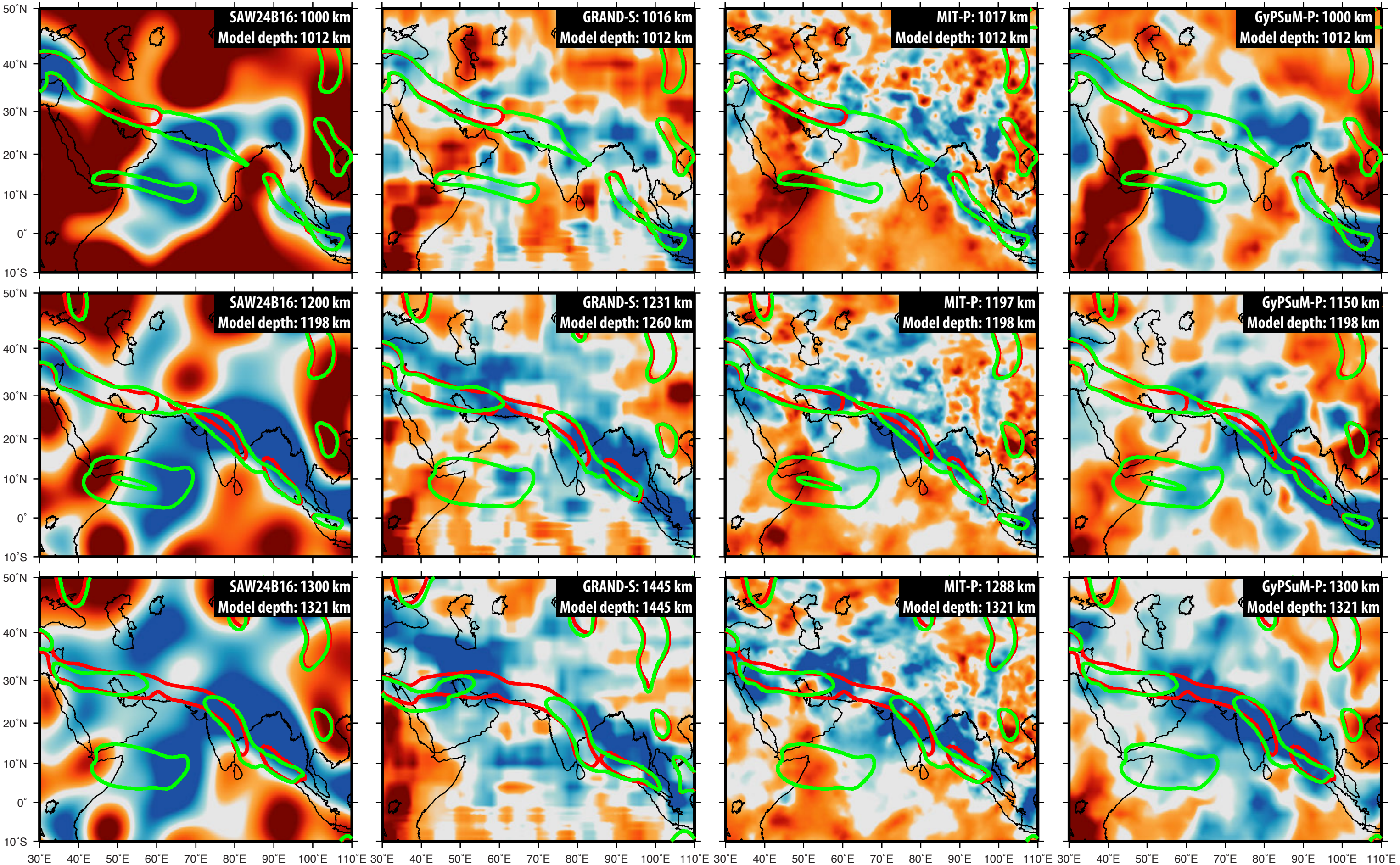
SAW24B16: 1000 km
Model depth: 1012 km
GRAND-S: 1016 km
Model depth: 1012 km
MIT-P: 1017 km
Model depth: 1012 km
GyPSuM-P: 1000 km
Model depth: 1012 km
SAW24B16: 1200 km
Model depth: 1198 km
GRAND-S: 1231 km
Model depth: 1260 km
MIT-P: 1197 km
Model depth: 1198 km
GyPSuM-P: 1150 km
Model depth: 1198 km
SAW24B16: 1300 km
Model depth: 1321 km
GRAND-S: 1445 km
Model depth: 1445 km
MIT-P: 1288 km
Model depth: 1321 km
GyPSuM-P: 1300 km
Model depth: 1321 km
50°N
40°N
30°N
20°N
10°N
0°
10°S
30°E
40°E
50°E
60°E
70°E
80°E
90°E
100°E
110°E

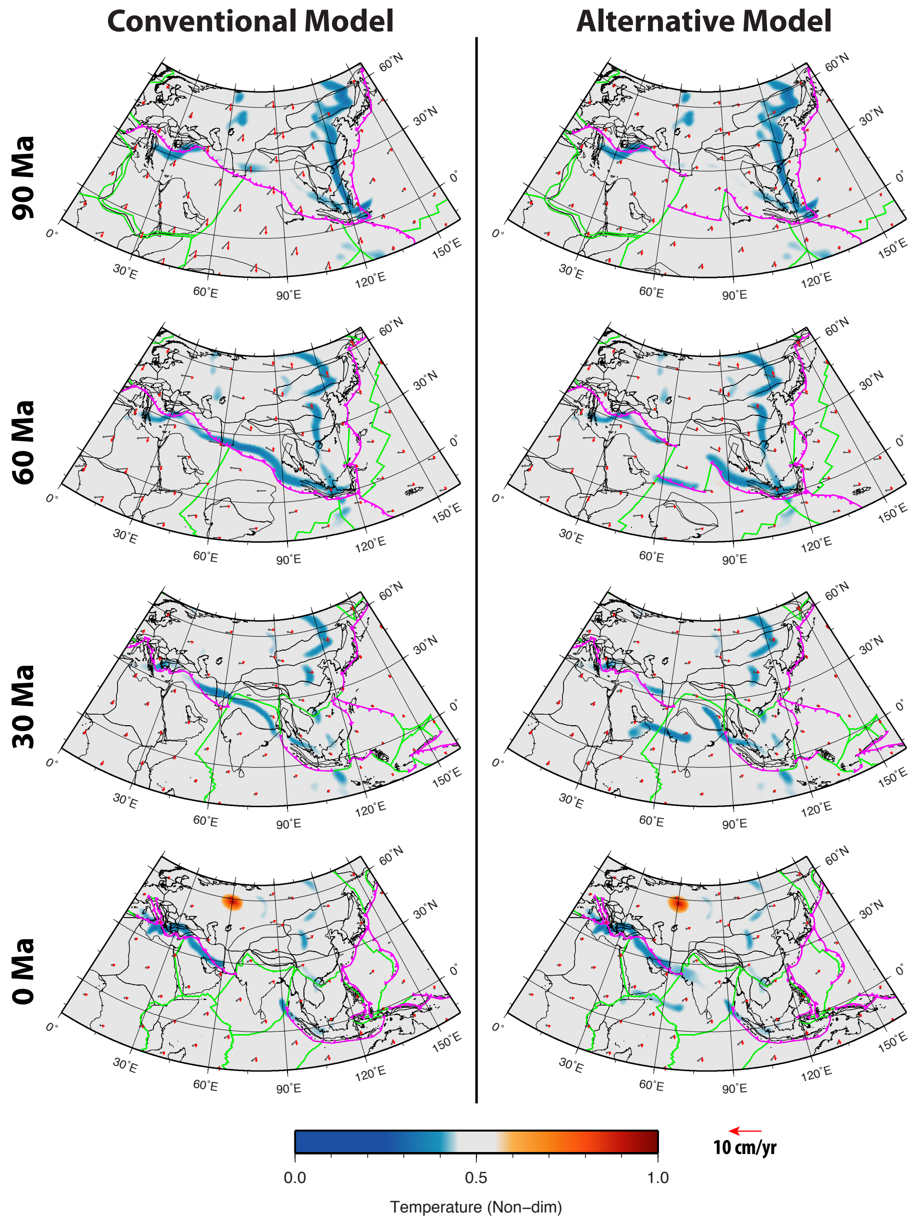

Conventional Model
Alternative Model
90 Ma
60 Ma
30 Ma
0 Ma
60°N
30°N
0°
0°
30°E
60°E
90°E
120°E
150°E
0.0
0.5
1.0
Temperature (Non–dim)
10 cm/yr